UCRL- 100651
PREPRINT

RECENT ADVANCES TO NEC: APPLICATIONS AND VALIDATION

G. J. Burke

This paper is being prepared for
submittal to the Modern Antenna Design
Using Computers and Measurement
Application to Antenna Problems of Military Interest
Ankara, Turkey
October 19-20, 1989

March 3, 1989

DISCLAIMER

RECENT ADVANCES TO NEC: APPLICATIONS AND VALIDATION *

G. J. Burke
Lawrence Livermore National Laboratory
P.O. Box 5504, L-156, Livermore, CA 94550

ABSTRACT

Capabilities of the antenna modeling code NEC are reviewed and results are presented to illustrate typical applications. Recent developments are discussed that will improve accuracy in modeling electrically small antennas, stepped-radius wires and junctions of tightly coupled wires, and also a new capability for modeling insulated wires in air or earth is described. These advances will be included in a future release of NEC, while for now the results serve to illustrate limitations of the present code. NEC results are compared with independent analytical and numerical solutions and measurements to validate the model for wires near ground and for insulated wires.

1. INTRODUCTION

Computer modeling of antennas, since its start in the late 1960's, has become a powerful and widely used tool for antenna design. Computer codes have been developed based on the Method of Moments, Geometrical Theory of Diffraction, or integration of Maxwell's equations. Of such tools, the Numerical Electromagnetics Code – Method of Moments (NEC) [1] has become one of the more widely used codes for modeling resonant sized antennas. There are several reasons for this, including the systematic updating and extension of its capabilities, extensive user-oriented documentation and accessibility of its developers for user assistance. The result is that there are estimated to be several hundred users of various versions of NEC world wide.

NEC has been under development for more than ten years (in earlier forms it was known as BRACT and AMP.) It is a hybrid code which uses an electric field integral equation to model wire-like objects and a magnetic field integral equation to model closed surfaces with time harmonic excitation. NEC is commonly applied to modeling antennas in VLF to VHF applications on ships, vehicles or on the ground. It includes a number of features for efficient modeling of antennas and scatterers in their environments including antennas interacting with or buried in a finitely conducting ground. Recent work on NEC has added a capability for modeling insulated wires in the air or ground and improved accuracy for electrically small antennas and the treatment of an abrupt change in wire radius.

We will review the current status of NEC and discuss recent enhancements and new developments. Some typical results and validation examples are included.

2. THE BASIC MODELING APPROACH

NEC combines an electric-field integral equation (EFIE) for wires and a magnetic-field integral equation (MFIE) for surfaces to model complex structures. Each equation has advantages for particular structure types. The EFIE is well suited for thin wires with small or vanishing conductor volume, while the MFIE, which fails for thin wires, is more attractive for closed, voluminous structures, especially those having large smooth surfaces. The EFIE can also be used to model surfaces and is preferred for thin structures where there is little separation between a front and back surface. Although the EFIE is specialized to thin wires in NEC, it can be used to represent surfaces as wire grids. Grid models are often more accurate for far-field quantities than for surface fields or currents, however. For a structure containing both wires and surfaces the EFIE and MFIE are coupled, as was described by Albertsen, Hansen and Jensen in [2]. A derivation of the EFIE and MFIE used in NEC is given by Poggio and Miller in [3].

The thin wire approximation is applied to the EFIE to reduce it to a scalar integral equation. The basic approximations are to neglect transverse currents and transverse variation of the axial current on the wire, and to enforce the boundary condition on electric field in the axial direction only. In NEC, the current is lumped as a filament on the wire axis and the boundary condition is enforced on the wire surface to facilitate evaluation of the kernel. These approximations are valid as long as the wire radius is much less than the wavelength and much less than the wire length. An alternate kernel for the EFIE, based on an extended thin-wire approximation in which the current is a tubular distribution on the wire surface, is also included for wires having too large a radius for the thin-wire approximation

* Work performed under the auspices of the U S. Department of Energy by the Lawrence Livermore National Laboratory under Contract W-7405-Eng-48.

[4]. With the thin-wire approximation, the EFIE for a wire with radius $a(s)$ becomes

$$-\hat{s}\cdot\vec{E}^i(\vec{r}) = \frac{-j\eta}{4\pi k}\int_C I(s')\left(k^2\hat{s}\cdot\hat{s}' - \frac{\partial^2}{\partial s\partial s'}\right)g(\vec{r},\vec{r}')\,ds', \qquad \vec{r}\in C(s) \tag{1}$$

where

$$g(\vec{r},\vec{r}') = \exp(-jkR)/R, \qquad R = [|\vec{r}-\vec{r}'|^2 + a^2(s)]^{1/2}$$
$$k = \omega(\mu_0\epsilon_0)^{1/2}, \qquad \eta = (\mu_0/\epsilon_0)^{1/2}.$$

I is the induced current, $\vec{E}^i$ is the exciting field, $\hat{s}$ and $\hat{s}'$ are unit vectors tangent to the wire at s and s', and $\vec{r}$ and $\vec{r}'$ are vectors to the points s and s' on the wire contour C.

The MFIE for a closed surface S is

$$-\hat{n}(\vec{r})\times\vec{H}^i(\vec{r}) = -\frac{1}{2}\vec{J}_s(\vec{r}) + \frac{1}{4\pi}\int_S \hat{n}(\vec{r})\times\left[\vec{J}_s(\vec{r}')\times\nabla' g(\vec{r},\vec{r}')\right]dA', \qquad \vec{r}\in S \tag{2}$$

where $\hat{n}(\vec{r})$ is the unit vector normal to the surface at $\vec{r}$, $\vec{H}^i$ is the exciting magnetic field and $\vec{J}_s$ is the surface current. Eq. (2) is derived from the condition that magnetic field is zero inside a perfectly conducting solid, with a jump of $\vec{J}_s\times\hat{n}$ at the surface. Hence it is valid only for a closed perfectly conducting shell. Eq. (2) is separated into coupled scalar integral equations for components of the surface current. For models involving both wires and surfaces the electric field due to surface currents is included in the right-hand side of Eq. (1) and the magnetic field due to wires is included in the right-hand side of Eq. (2) leading to coupled integral equations for the currents.

While Eqs. (1) and (2) apply to an antenna in free space, they are easily extended to an infinite dielectric or conducting medium by replacing ϵ_0 and μ_0 by ϵ and μ of the medium. When the antenna is located near a ground plane, the right-hand sides of Eqs. (1) and (2) are modified to include the increment in the field of the source current due to the interface, either using an image or (for wires only in NEC–3) the Sommerfeld-integral solution for a point source near the interface.

The integral equations (1) and (2) are solved numerically by a form of the method of moments, which involves expanding the unknown current in a summation of basis functions and enforcing equality of weighted integrals of the fields to reduce the integral equation to a matrix equation [5]. The weighting functions for both wires and surfaces are chosen to be delta functions, resulting in a point sampling of the fields known as the collocation method. Wires are divided into short straight segments with a sample point at the center of each segment, while surfaces are approximated by a set of flat patches or facets with a sample point at the center of each patch.

Delta functions are also used as the current expansion functions on surfaces. For the MFIE this elementary Galerkin's method has been found to provide good accuracy on large smooth surfaces. Due to the nature of the integral-equation kernels, however, the choice of current expansion functions is more critical in the EFIE than in the MFIE.

The expansion functions for the current on wires are chosen so that the total current on segment number j has the form

$$I_j(s) = A_j + B_j\sin k_s(s-s_j) + C_j\cos k_s(s-s_j), \qquad |s-s_j| < \Delta_j/2 \tag{3}$$

where s_j is the value of s at the center of segment j and Δ_j is the length of segment j. The factor k_s is normally equal to the wave number in the medium containing the wire. This expansion was first used by Yeh and Mei [6] and has been shown to provide rapid solution convergence. In NEC, the constants in Eq. (3) are chosen so that the basis functions are generalized B-splines extending over three segments (or more at multiple wire junctions) and constructed from the three-term sinusoidal function.

Two of the three constants in Eq. (3) are eliminated by continuity conditions on current and charge at the segment ends. Current is continuous or satisfies Kirchhoff's current law at multiple wire junctions. Charge is continuous on uniform wires. At a junction where the wire radius changes, the linear charge density (or $\partial I/\partial s$) on the wire with radius a_i is made proportional to

$$\Psi_i = \left[\ln\left(\frac{2}{ka_i}\right) - 0.5772\right]^{-1}. \tag{4}$$

This condition on charge was derived in [7] by analysis of a wire with tapered radius, and hence is often called the Wu-King condition. On a wire passing from air into ground, the charge is discontinuous by the ratio of media permittivities [8]. Expressions for the basis functions that result from applying these conditions on current and charge are included in [1]

Where a wire connects to a surface, a more realistic representation of the surface current is needed than the delta-function expansion normally used with the MFIE. The treatment used in NEC is similar to that used by Albertson et al. [2]. In the region of the wire connection, the surface current includes a singular component with the form $\vec{\rho}/\rho^2$, where $\vec{\rho}$ is the the surface vector from the attachment point, as well as a continuous function providing interpolation to the current on adjacent patches.

As a result of the continuity conditions on current and charge there remains one unknown associated with each basis function to be determined by solving the electromagnetic interaction equations. Enforcing appropriate conditions on the current and charge results in rapid convergence of the solution. The danger is that the conditions may be inappropriate under some conditions, as may occur in NEC at a change in wire radius and at junctions of closely spaced wires. The result is then slower convergence. More accurate conditions for these cases are being developed, as discussed in Section 4.

3. CAPABILITIES OF NEC

Two versions of NEC are currently being released: NEC–2 which has no distribution restrictions and NEC–3 which is classified as Defense Critical Technology, and hence can be released only to DoD agencies and contractors. Foreign release of NEC–3 requires specific DoD approval. The only difference in the capabilities of these codes is that NEC–3 can model wires that are buried or penetrate from air into the ground, while NEC–2 is limited to antennas in free space or above a ground plane. The capabilities of these codes are summarized below.

3.1 Source Modeling

A voltage source on a wire may be modeled by an applied field on a segment or a discontinuity in charge between segments. The charge discontinuity, or "bicone" source model yields a more localized excitation than the field over a segment, but it is accurate only for small wire radius [9]. Alternatively, a structure may be excited by a plane wave with linear or elliptic polarization or by the near field of an infinitesimal current element.

3.2 Nonradiating Networks, Transmission Lines and Loading

Nonradiating two port networks and transmission lines may connect points on wires. These are modeled by constructing a driving-point admittance matrix from the admittance matrix of the entire structure to avoid modifying the larger matrix. Lumped or distributed RLC loads may be specified on wires. Also, the conductivity of a round wire may be specified and the impedance computed taking account of skin depth.

3.3 Ground Effects

Three options are available for an antenna in or near the ground. A perfectly conducting ground is modeled by including the image field in the kernel of the integral equation. This doubles the time to compute the interaction matrix. An approximate model for an antenna over a finitely conducting ground uses the image modified by Fresnel plane-wave reflection coefficients. This approximation is usable for antennas at least 0.1 to 0.2 wavelengths above the ground and doubles the time to fill the matrix.

NEC–3 includes an accurate treatment for wire structures above, below, or penetrating the ground surface. The solution is based on the Sommerfeld-integral formulation for the field near the interface. For the moment-method solution, the field values are obtained by table lookup and parameter estimation involving a model for the functional behavior of the field transmitted across the interface. The current expansion is modified to account for the discontinuity in charge on a wire penetrating the interface. This numerical treatment for buried wires is described in [8]. NEC–2 includes a similar ground model limited to wires above the ground.

Over ground, NEC will compute the radiated space wave, with direct and reflected rays, and can also include the surface wave. A cliff or abrupt change in ground parameters is treated by computing the reflected ray for the appropriate ground parameters and height at the reflection point, but without including diffraction. Hence at grazing angles to the ground, since the reflection point is at an infinite distance, only the outer medium affects the field. The inner medium is always used in computing the antenna currents. Also, no model for a cliff is available when the surface wave is computed. Options for a more complete treatment of a cliff are discussed in Section 4.5.

3.4 Efficient Solution Methods

The matrix equation that results from the moment method is solved by LU decomposition, with the factors saved for reuse when the excitation or other parameters that do not alter the matrix are

changed. Rotational symmetry or reflection symmetry in one to three planes can be used to reduce the times to fill and to factor the matrix. New wires or surfaces may be added to a structure for which the matrix has already been computed, factored and saved on a file. The new solution is found from the self and mutual interaction matrices through a partitioned-matrix algorithm with no unnecessary repetition of calculations for the basic structure. This feature can be used to take advantage of symmetry in a portion of a structure to which unsymmetric parts connect or interact.

3.5 Input

A user-oriented input scheme permits defining straight wires, arcs, and surfaces. Shifts, rotations, and reflections can be used in building complex structures. Electrical connections are determined in the program by searching for wire ends and patch centers that coincide. A solution can be repeated for modified model parameters (transmission lines, loading, ground, etc.) in the input sequence without respecifying parameters that are not changed.

3.6 Output

Output may include current, charge density on wires, input impedance, admittance, input power, ohmic loss and efficiency. For transmitting antennas, radiated field and power, power gain, directive gain, average gain and ground-wave field are available. Near $\vec{E}$ and $\vec{H}$ can be computed at points on or off of the antenna. Receiving patterns and scattering cross sections are available with incident field excitation.

3.7 Modeling Guidelines

There are a number of rules that must be followed in specifying the model in order to obtain accurate results from a code such as NEC. Unfortunately many of these rules can be ignored and the code will still give results — usually wrong. Hence a user should become familiar with the modeling guidelines before attempting to use the code. Some of the guidelines are summarized below.

For accurate results, the lengths of wire segments should be less than about 0.1 λ. Longer segments up to about 0.14 λ may be acceptable on long, straight wires or noncritical parts of a structure, while shorter segments, 0.05 λ or less, may be needed in modeling critical regions of an antenna. There is also a minimum segment length set by the computational precision. With seven place precision, common on 32-bit computers, the minimum segment length is about $10^{-4}\lambda$. In double precision the minimum length is about $10^{-8}\lambda$. The restrictions on minimum segment length will be relaxed in a future version of the code, as discussed in Section 4.1.

The wire radius a relative to λ is limited by approximations used in the kernel of the EFIE. Two options are available in NEC: the thin-wire kernel (TWK) and the extended thin-wire kernel (ETWK). With the ETWK the ratio of segment length to radius can be as small as 0.5 before instabilities appear in the solution, while with the TWK the limit is 2. In either case, only currents in the axial direction on a segment are considered, and there is no allowance for variation of the current around the wire circumference. Also, the ETWK, when it is selected, works only on straight sections of wire. The acceptability of these approximations depends on both the value of a/λ and the tendency of the excitation to produce circumferential currents or current variation. The capacitive effect of a step in radius, and consequent shortening of the electrical length, is not modeled accurately in the present NEC. If a discontinuous radius must be modeled it is best to keep the ratio of radii less than two, and to use segments as long as possible at the discontinuity. A new model for a stepped-radius wire is described in Section 4.3.

Electrically small loops present special accuracy problems. In single precision the minimum loop circumference is about 0.07λ while in double precision it is about $3(10^{-4})\lambda$. These limits can be removed, as described in Section 4.2, by including loop basis and weighting functions on each small loop. This capability is not yet in the released version of NEC, however. For a loop over a finitely conducting ground the solution fails when the loop size is somewhat less than resonant. Hence small loops over ground cannot presently be modeled.

Due to the nature of the MFIE, surfaces modeled with patches must be closed. A reasonable maximum for the area of a surface patch on a smooth surface appears to be 0.04 square wavelengths.

An important consideration in using NEC is the solution time versus model size since this may limit the amount of detail that can be modeled and the segment and patch densities. For a model using N wire segments, the solution time in seconds on a CDC 7600 computer is approximately

$$T = 3(10^{-4})kN^2/M + 2(10^{-6})N^3/M^2 \tag{5}$$

where M is the number of degrees of symmetry and k is 1 for free space or any infinite medium, 2 for an antenna over perfectly conducting ground or real ground modeled with the reflection coefficient approximation, and 4 to 8 for the accurate (Sommerfeld integral) treatment of finitely conducting ground. The first term in Eq. (5) is the time to fill the interaction matrix and the second term is the time for the LU decomposition.

For a model using N_p patches, the solution time is about

$$T = (10^{-5})k(2N_p)^2/M + 2(10^{-6})(2N_p)^3/M^2$$

since two rows and columns in the matrix are associated with each patch. The reduced time factor for filling the matrix, due to the delta-function current expansion, is one attractive feature of this solution method. A more complete relation for running time is contained in [1], Part III.

When the Sommerfeld ground treatment is used, a fixed time of about 15 seconds on a CDC 7600 computer is needed to generate the interpolation tables. The tables depend only on the ground parameters and frequency, however and can be saved for reuse in any case in which these parameters are the same.

4. NEW DEVELOPMENTS IN NEC

Although the present NEC offers a reasonably versatile and accurate modeling capability, there are a number of situations that may not be handled accurately. Recent work on the thin-wire code has increased the precision and model accuracy for electrically small antennas and developed more accurate treatments for wires with discontinuous radius and junctions of tightly coupled wires. Also, a model for insulated wires has been added to a version of NEC–3. These developments, which will be included in future versions of NEC, are described below.

4.1 Enhanced Precision for Electrically Small Structures

NEC was originally developed on computers having 60-bit numerical precision, so little attention was given to preserving numerical accuracy. Problems may become apparent when the code is run on computers with 32-bit single precision. Precision loss is particularly severe when modeling electrically small antennas, and often forces the use of double precision. Hence we have NEC–2S and NEC–3S codes in single precision and NEC–2D and NEC–3D in double precision on DEC/VAX computers. Double precision, of course, increases the storage requirement and more than doubles the solution time, so some large VLF models are run in single precision because double is unaffordable. Problems in modeling electrically small antennas can be divided into those that affect any small structure and those that occur with electrically small loops. Changes to correct low frequency problems other than loops are described in [10] and are summarized below.

To improve the accuracy of the single precision NEC, we have revised the code for evaluation of the basis functions and fields. A basic problem at low frequencies is the cancellation between the constant and $\cos(k_s s)$ components in Eq. (3). In the new code, the same spline basis functions are used but they are evaluated in the form

$$I_j(s) = A'_j + B_j \sin k_s(s - s_j) + C_j[\cos k_s(s - s_j) - 1], \qquad |s - s_j| < \Delta_j/2$$

over each segment. To permit modeling extremely short segments, it was also necessary to arrange the order of calculation to avoid overflow or underflow of intermediate results in evaluating the spline functions.

Precision loss is also a problem in the field evaluation. The present code evaluates the electric field of each segment, including the contributions of point charges at the segment ends that result from the current dropping abruptly to zero. These point-charge terms dominate the field of a segment at low frequencies but are cancelled by adjacent segments when current is continuous. Since continuity of current is ensured in the current expansion, these terms can be dropped from the field evaluation to preserve accuracy.

The fields due to $\sin(k_s s)$ and $\cos(k_s s)$ currents are evaluated from exact closed-form expressions when k_s is equal to the wave number k in the surrounding medium, while the field of a constant current involves an integral that must be evaluated numerically or by approximation. Even with the point-charge terms removed, the field equations suffer severe cancellation that necessitates the use of series expansions for small kR, R much greater than segment length and for ρ much less than z, where ρ and z are the coordinates of the evaluation point relative to a segment on the z axis and $R = (\rho^2 + z^2)^{1/2}$.

To compute the input resistance of small antennas it was necessary to maintain the accuracy of the real part of the electric field although, for some components, it decreases faster than the imaginary part by a factor of $(kR)^3$.

These changes have been made in a code called NEC3VLF. This is an interim code to which additional changes are being made. However, a comparison of results from NEC–3S, NEC–3D and NEC3VLF reveals some of the limitations of NEC–3 and the potential improvements. One way to determine the low frequency limit of the code is to decrease the frequency until the solution obviously fails. Such results are shown for a dipole in Fig. 1. NEC–3S fails at a point that could cause problems in modeling practical VLF antennas. NEC–3D could handle most practical applications, but at the expense of increased solution time and storage. NEC3VLF is limited only by the underflow of the conductance and is also faster than NEC–3S due to a faster series approximation for the integral of $\exp(-jkR)/R$.

The solution in NEC–3S can also become inaccurate for a fixed length dipole as the number of segments is increased. This problem has been corrected in NEC3VLF as shown in Fig. 2.

4.2 Electrically Small Loops

The difficulty in modeling loops can be seen when the electric field of a wire is written as

$$\vec{E}(\vec{r}) = \frac{-j}{4\pi\omega\epsilon}\left[\nabla\int_\ell \frac{e^{-jkR}}{R}\frac{\partial I(s')}{\partial s'}\,ds' + k^2\int_\ell \frac{e^{-jkR}}{R}\hat{s}'I(s')\,ds'\right]. \tag{6}$$

As frequency is reduced the field of a spline basis function is dominated by the first term in Eq. (6), while the second term decreases as ω^2. However, the sum of equal basis functions around a loop is a constant current with zero derivative, so that the first term in (6) vanishes. Thus the sum of matrix columns representing the spline basis functions around the loop is much less than the individual columns, indicating an ill-conditioned matrix. With unlimited precision the basis functions used in NEC could handle arbitrarily small loops. In single precision, however, accuracy is quickly lost as frequency is reduced.

The problem is still worse when a loop is excited by coupling to a source such as a dipole with large concentrations of charge. The loop current is then determined by the line integral around the loop of the field of the dipole. At low frequency the dipole field is dominated by the gradient term in Eq. (6) which must vanish in the line integral around the closed loop. Hence the sum of matrix rows representing segments of the loop is much less than the individual rows. This problem in NEC is worse than the degeneracy of the basis function fields since the integral of $\vec{E}$ around the loop is sampled in a relatively crude form as the sum of the fields at the centers of segments. Hence, use of double precision does not help the solution for a loop coupled to charge, and large incorrect loop currents can result. This problem may occur whenever a wire end with high charge density is near a small loop.

The problems in modeling small loops can be fixed, as shown in [11], by changing the current expansion to include a function that is constant around the loop, and also using one constant weighting function. This use of loop basis and weighting functions was suggested by D. R. Wilton [12] for a Galerkin moment-method code similar to MININEC [13]. On a small loop, the loop basis function represents the dominant part of the solution while the remaining spline functions account for the small variations of the current. Loop basis functions can also be used on electrically large loops since replacing one spline basis function with a constant loop function does not change the space spanned by the basis. The constant function is exactly equal to an equal-amplitude sum of the spline functions.

In implementing the loop weighting function, the gradient of the scalar potential is dropped from the field evaluation since it must vanish when integrated around a closed loop. With an accuracy and effort compatible with the point matching normally used in NEC, the line integral of $\vec{E}$ around the loop is then approximated from the sum of the vector potentials at the centers of segments. The loop-weighted equation replaces one of the point-matched equations, typically for the same segment on which the spline basis function was removed for the loop basis function. This replacement can introduce some asymmetry on an otherwise symmetric loop, but such effects are within the bounds of convergence of the solution.

A tricky problem in implementing loop basis and weighting functions is that of locating all loops in a complex wire structure. Code has been developed for this task, but it cannot yet handle completely general wire structures.

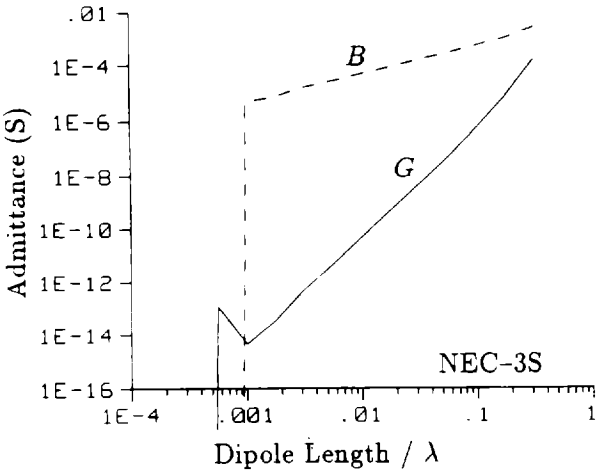

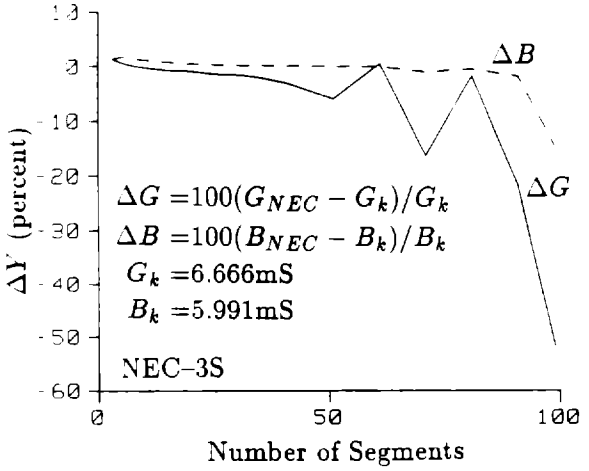

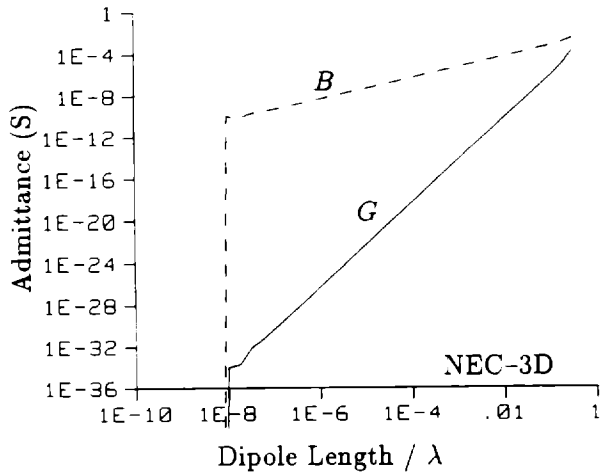

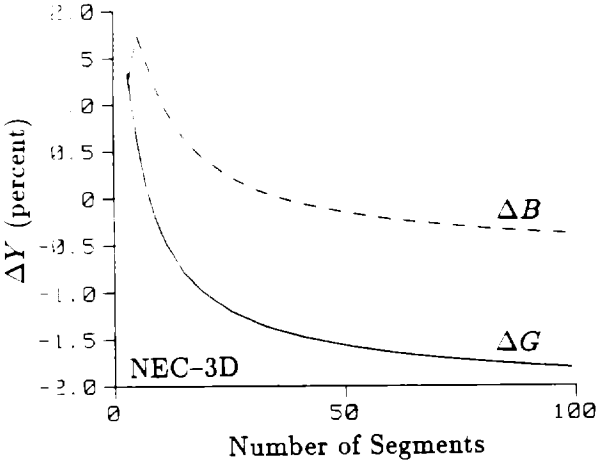

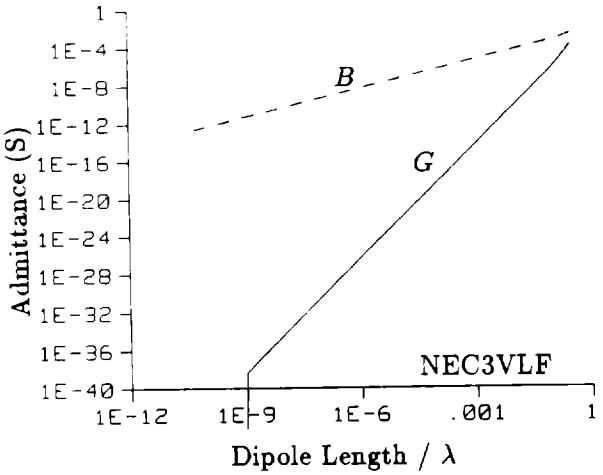

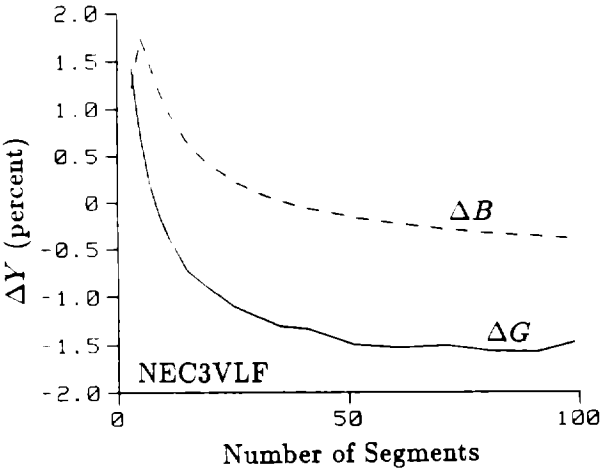

Fig. 1. Input admittance of a dipole antenna computed by NEC-3S, NEC-3D and NEC3VLF. The dipole was modeled with 9 segments and the ratio of radius to dipole length was 10^{-3}. Solution failure is shown by the deviation from the low frequency asymptotic behavior.

Fig. 2. Input admittance of a $\lambda/2$ dipole antenna computed by NEC-3S, NEC-3D and NEC3VLF with varying number of segments. The difference from the King-Middleton result ($G_k + jB_k$) is plotted. The ratio of dipole radius to length is $4.5(10^{-5})$ (Ω=20).

Validation of results for small loops is more difficult than for open wires since the double precision NEC-3, which was used as a standard for dipoles, may give the same wrong results as single precision for loops. The most useful checks on the solution for loops were found to be convergence as the number of segments is increased, the average gain as a check of radiated power versus input power and correction of obviously wrong results for decreasing frequency.

Results for a wire loop containing a voltage source are shown in Fig. 3. In this case the VLF limitation is due to the degeneracy of the fields of the spline basis functions rather than the field sampling. Use of double precision in NEC-3 does reduce the low frequency limit in this case at the expense of

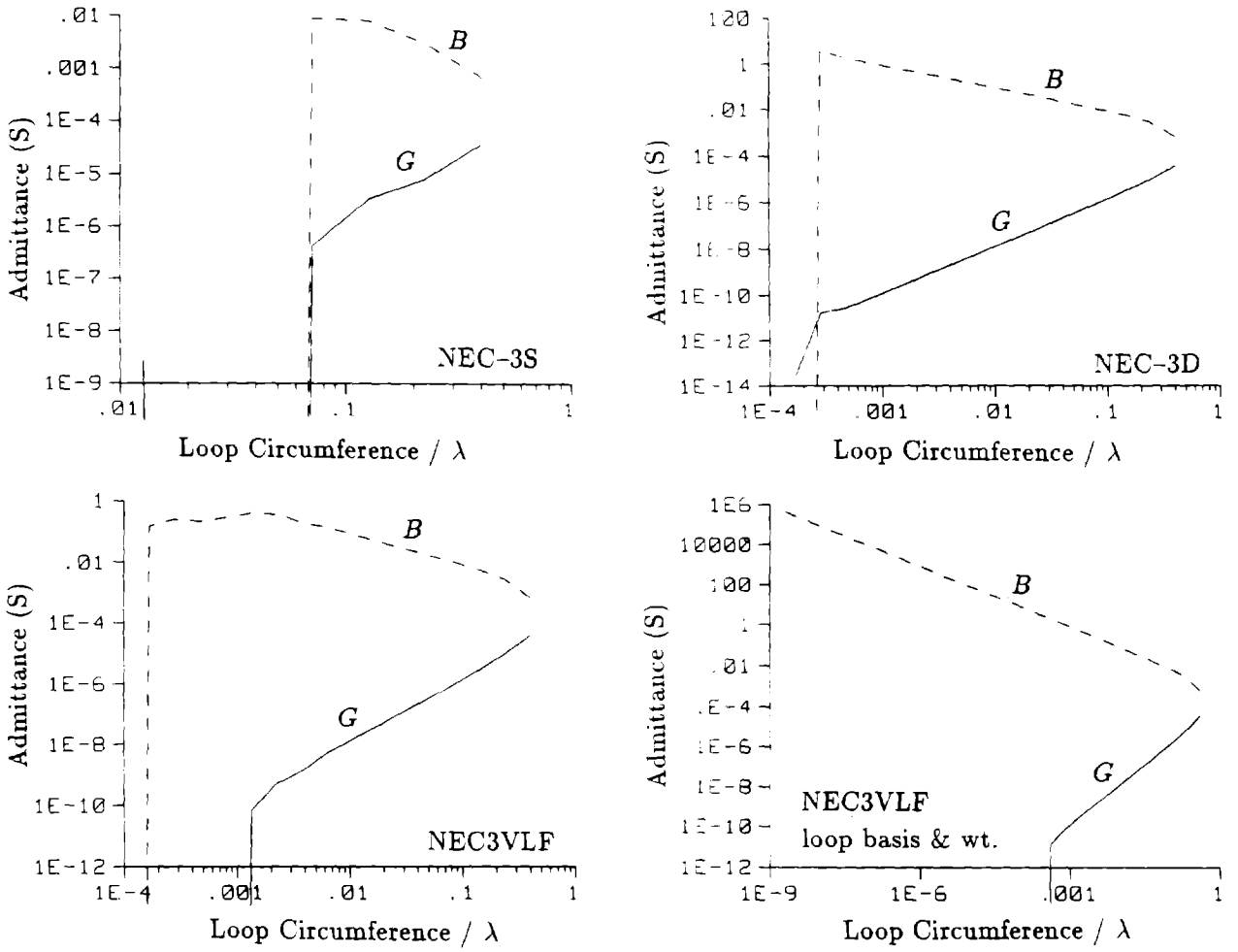

Fig. 3. Input admittance of a loop antenna computed by NEC-3S, NEC-3D and NEC3VLF with and without loop basis and weighting functions. The loop was modeled with 22 segments and the ratio of wire radius to loop radius was 0.042. Solution failure is shown by deviation from the low frequency asymptotic behavior.

increased computation time and storage. NEC3VLF with loop basis and weighting functions gives the correct behavior for input conductance to about the same limiting frequency as double precision NEC-3. The new code appears to have no limitation for computation of input susceptance. Hence after the solution for conductance fails the correct value can be determined by integrating the far-field power on an otherwise lossless antenna. The reason for failure of the conductance at a circumference of about $4(10^{-4})\lambda$ has not been isolated, but may be difficult to avoid given the difference in magnitude from the susceptance.

An example of loops coupled to a charge concentration is provided by the stub antenna on a wire-grid fin, shown in Fig. 4. The NEC-3D result has an incorrect clockwise circulation of current on the grid while NEC3VLF with loop basis and weighting functions produced a uniform flow of current toward the stub. As frequency is reduced the incorrect circulating current from NEC-3 grows as f^{-2} relative to the stub current while the NEC3VLF result remains stable. Results for input impedance and average gain of this structure with decreasing frequency are shown in Table 1. The last two frequencies resulted in division by zero in NEC-3S. The difference of the average gains from the correct value of 1.0 was found to be due to extraneous input power at small, but not negligible, voltages across the segments on which match points were dropped. These errors are within acceptable bounds for most applications, however. The minimum frequency at which NEC-3 yields acceptable accuracy will decrease as the wire end, with its charge concentration, is moved further from the loop.

The severity of the errors with the standard NEC solution for small loops would seem to make the use of loop basis and weighting functions essential. However, the difficulties of locating small loops and of implementing this treatment for arbitrary structures including a ground plane may delay its use.

4.3 Modeling Stepped-Radius Wires and Junctions

The problems with the present NEC model for a stepped-radius wire can be seen by comparing the solution for charge with that from an accurate solution of the surface model. Glisson and Wilton have

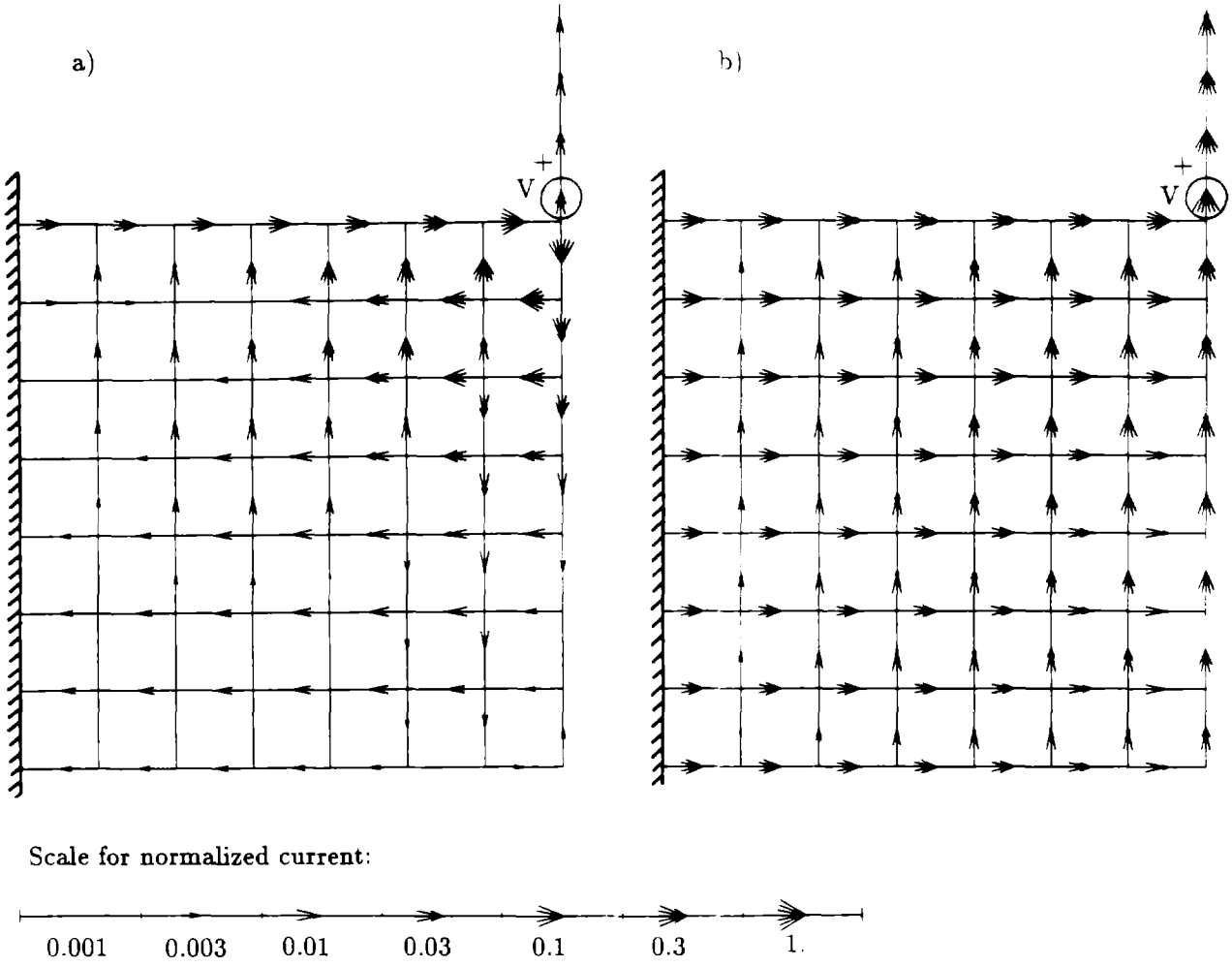

Fig. 4. Imaginary part of current on a wire grid fin with stub antenna. The fin is 0.014λ high and connects to a perfectly conducting ground plane. The source is one volt at the base of the stub and current is normalized by I_{max}; a) NEC–3D result with incorrect grid current, I_{max} = 2.62 mA; b) NEC3VLF with loop basis and weighting functions, I_{max} = 0.10 mA.

Table 1. Input impedance and average gain of the wire grid with stub antenna from NEC–3 in single precision (NEC–3S) and double precision (NEC–3D) and NEC3VLF with loop basis and weighting functions. Δ is the width of the openings in the mesh.

	NEC–3S			NEC–3D			NEC3VLF		
Δ/λ	R (ohms)	X (ohms)	$\bar{G}$	R (ohms)	X (ohms)	$\bar{G}$	R (ohms)	X (ohms)	$\bar{G}$
$2.(10^{-2})$	60.98	$-7.82(10^2)$	1.01	60.98	$-7.82(10^2)$	1.14	$5.91(10^1)$	$-8.00(10^2)$	0.93
$2.(10^{-3})$	0.60	$-9.38(10^3)$	0.30	$1.78(10^{-1})$	$-9.66(10^3)$	1.19	$1.65(10^{-1})$	$-9.80(10^3)$	0.92
$2.(10^{-4})$	-7.55	$-8.74(10^4)$	-10^{-4}	$1.76(10^{-3})$	$-9.67(10^4)$	5.66	$1.63(10^{-3})$	$-9.81(10^4)$	0.91
$2.(10^{-5})$	***	***	***	$1.75(10^{-5})$	$-9.67(10^5)$	484.	$1.63(10^{-5})$	$-9.81(10^5)$	0.91
$2.(10^{-6})$	***	***	***	$9.81(10^{-5})$	$-9.04(10^6)$	0.08	$1.63(10^{-7})$	$-9.81(10^6)$	0.91

shown in [14], by solution of a surface integral equation for the body of revolution, that the charge density at a step in radius is singular at the outer edge and goes to zero at the inner edge of the step, similar to the behavior of charge on an infinite wedge. If the sinusoidally varying charge density further from the step is extrapolated to the junction, their solution shows the discontinuity given by Eq. (4).

Similar, although probably less accurate, results can be obtained from NEC by modeling the stepped-radius wire as a cage of thin wires. Such a model is shown in Fig. 5 where twelve wires were used to model a monopole with the radius reduced by a factor of two. The monopole in Fig. 5 is viewed at one degree from end on, but is actually very thin relative to its length. As shown by A. Ludwig in [15], the error in modeling a thick wire as a cage of n thin wires is least when the radius of the thin wires is approximately equal to the radius of the thick wire divided by n. Since we did not

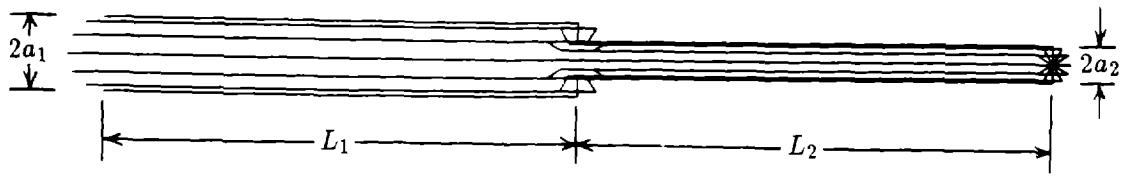

Fig. 5. A twelve-wire cage model of a monopole with stepped radius. The monopole is fed against a ground plane at its thick end. Dimensions are $a_1 = 0.00025\lambda$, $a_2 = 0.000125\lambda$ and $L_1 = L_2 = 0.125\lambda$.

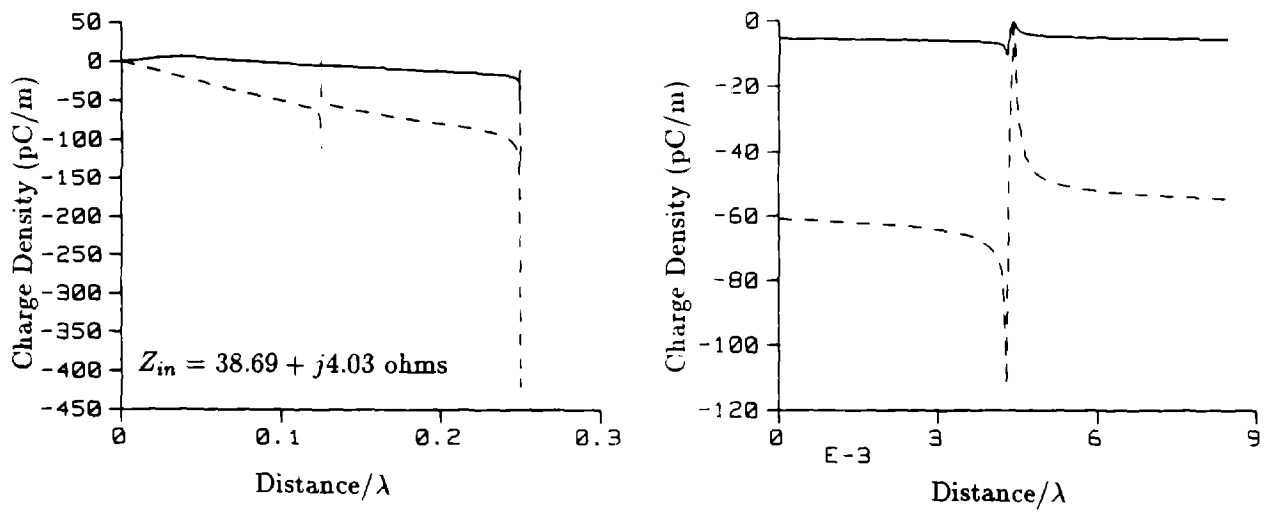

Fig. 6. Charge distribution determined by NEC for the twelve-wire model of a stepped-radius monopole; a) total charge density on the monopole, b) detail of charge density at the step in radius.

want to change the radius of the individual wires, an average radius of $(a_1 + a_2)/24$ was used. In order to resolve the behavior of charge at the step in radius and at the wire end, the short radial wires at these points were modeled with two segments each. The axial segments were tapered to have lengths equal to those of the radial segments at their connections. Results in Fig. 6 from the twelve-wire model show the behaviour of charge at the step and the wire end, and a displacement approximating Eq. (4) at larger distances from the step.

The NEC solution for the charge on the stepped-radius monopole modeled as a single wire is shown in Fig. 7. With segment lengths of $\Delta = 0.03125\lambda$ the discontinuity of Eq. (4) is evident in the charge, and the input impedance is in reasonable agreement with that obtained from the cage model in Fig. 6. However, when the segment lengths at the junction are reduced to $\Delta = 0.0005\lambda$ the charge becomes nearly continuous approaching the step. The discontinuity in charge that is enforced in the current expansion is still present, but it is evident only on the segments immediately adjacent to the step, where it is inappropriate due to the edge effects.

The convergence to continuous charge indicates a failure in the thin wire approximation as implemented in NEC. In NEC-3 and prior codes the current was treated as a filament on the wire axis with match points on the surface to avoid discontinuities in the current, and consequent point charges, at bends and steps in radius. Once the point charges have been dropped from the field evaluation, as discussed in Section 4.1, the current can be located on the wire surface without too much concern for maintaining physical continuity of the distribution. When current is located on the surface and match points on the axis, the solution for charge converges to approximately the discontinuity of Eq. (4) at points away from the edge effects.

Wire ends can then be closed by caps so that the boundary condition matched on the wire axis can represent an exact solution of the surface problem, in the sense of the extended boundary condition [16]. We have used a simple model for end caps, using flat caps with constant charge density that maintains continuity of current and charge with that on the wire. Hence, no new unknowns are introduced by the end caps. Caps were also included on voltage sources to prevent the source field from exciting the inside of the wire. The charge on the source caps is determined by the capacitance of the gap and the source voltage. Hence the field of this charge is added to the excitation vector on the right-hand side of the matrix equation.

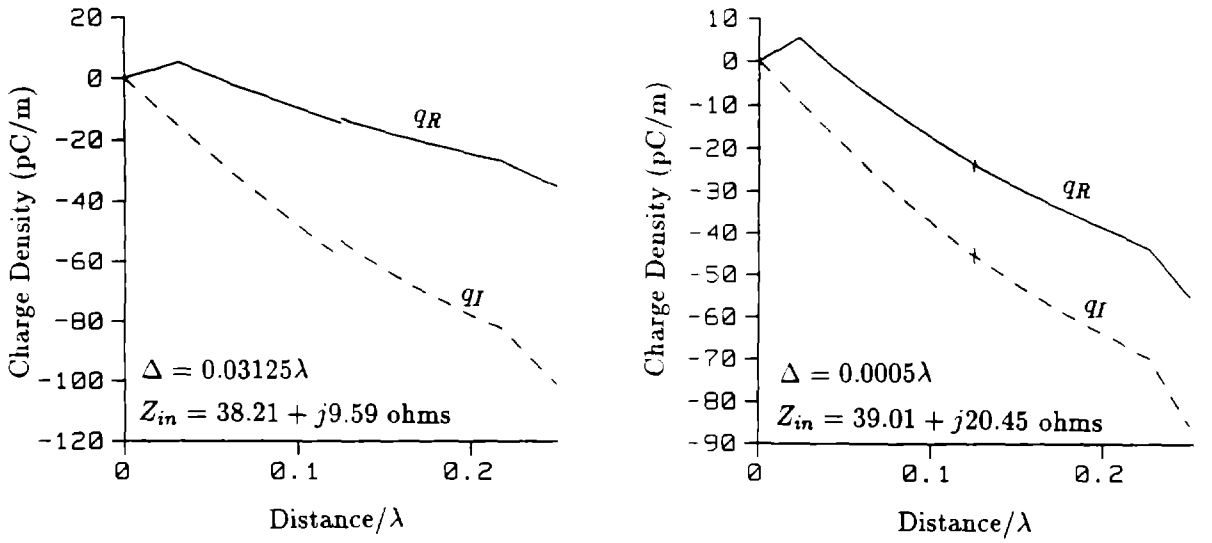

Fig. 7. NEC-3D solution for linear charge density on the monopole of Fig. 5 modeled as a single wire with segment length Δ at the step in radius. For $\Delta = 0.0005\lambda$ segment lengths were tapered for shorter segments at the junction.

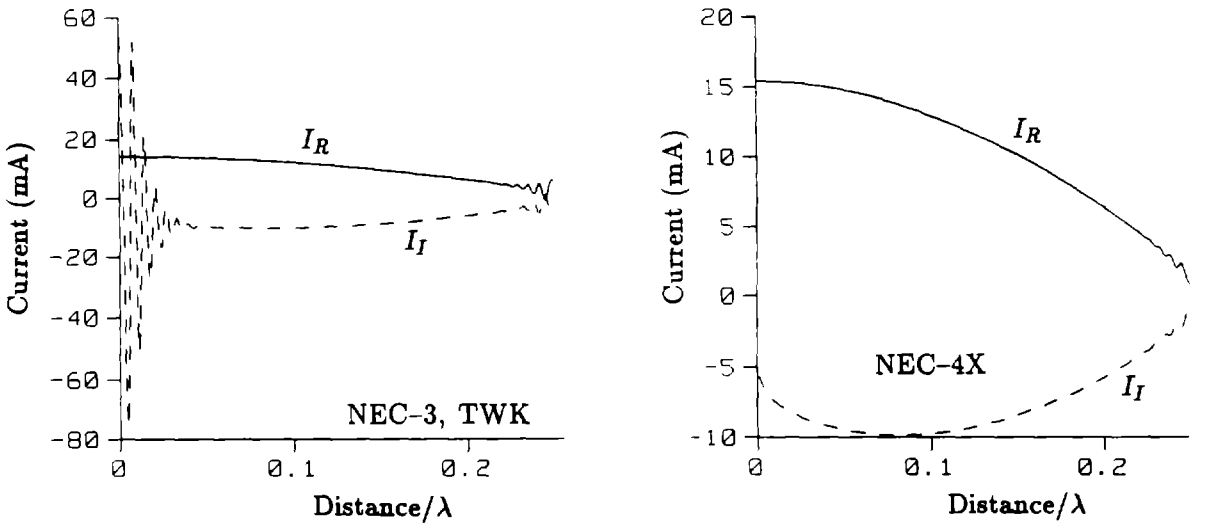

Fig. 8. Current on a $\lambda/4$ monopole excited by a 1 V source at its base, from NEC-3D and NEC-4X. The monopole had a radius of 0.01λ and was modeled with 80 segments.

A condition on charge density that takes into account the proximity of a step in radius and interaction of wires at a junction is determined with minimal computational overhead by executing a small moment-method solution. Any junction on which the charge cannot be determined as uniform due to symmetry is considered isolated from the rest of the structure with the wires extended to infinity away from the junction. An integral equation based on continuity of scalar potential is then solved to determine the distribution of charge. The charge is represented in a piece-wise linear expansion, with triangular basis functions and one semi-infinite basis function on each wire. A single half-triangle and the semi-infinite function were found to be sufficient for convergence.

The new code with the current on the wire surface, end caps, and the new condition on charge at a junction is, for now, called NEC-4X. The effect of including end caps on wire ends and voltage sources is shown in Fig. 8 where results of NEC-3 are compared with NEC-4X. The caps have a significant effect only when the segment length is on the order of the wire diameter or less. However, in view of their effectiveness for short segments, the ETWK will probably be dropped from the next version of NEC. We also plan to investigate the importance of closing the annular surface at a step in radius.

Results of NEC-3 and NEC-4X are compared with the surface solution of Glisson and Wilton for a stepped-radius wire in Fig. 9. The NEC models used relatively short segments at the step. Hence the NEC-3D result shows a large error in current and the nearly continuous charge density seen before. As

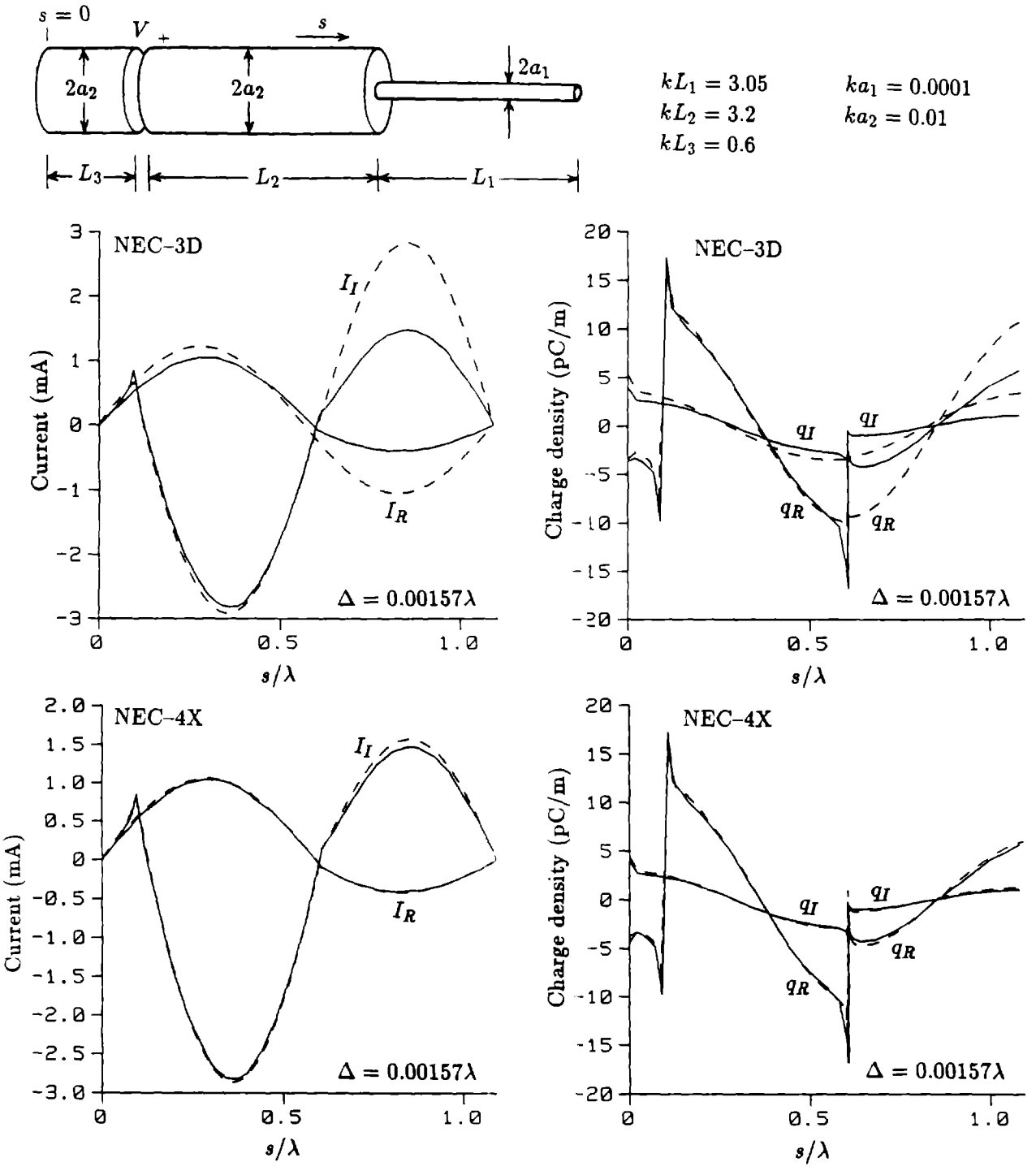

Fig. 9. Current and charge density on a stepped-radius wire. Results from Glisson and Wilton [14] (———) are compared with NEC-3D and NEC-4X (— — —).

the segment length at the step is increased the error in the NEC-3D result slowly decreases, while the NEC-4X result remains stable and in good agreement with the surface model.

An example of a junction of tightly coupled wires is found in a strip-line EMP simulator constructed from 18 wires as shown in Fig. 10. Results from NEC-3D and NEC-4X for the currents in the wires are shown in Fig. 11 when the line is driven by a one volt source at 4 MHz. NEC-3D is seen to produce nearly uniform currents while results of NEC-4X show larger currents, by nearly a factor of three, in the outer wires as reported from measurements [17]. The vertical component of electric field is compared with measurements in Fig. 12. The field from NEC-3D is too large by a factor of about two, while NEC-4X results are in better agreement with measurements. The results for E_z were numerically integrated from the ground plane to the center of the wire nearest the center plane at $x = 0$ m, $y = 0.02$ m. For a one volt source this integral resulted in 1.93 volts for NEC-3D and 1.05 volts for NEC-4X, further confirming the accuracy of NEC-4X.

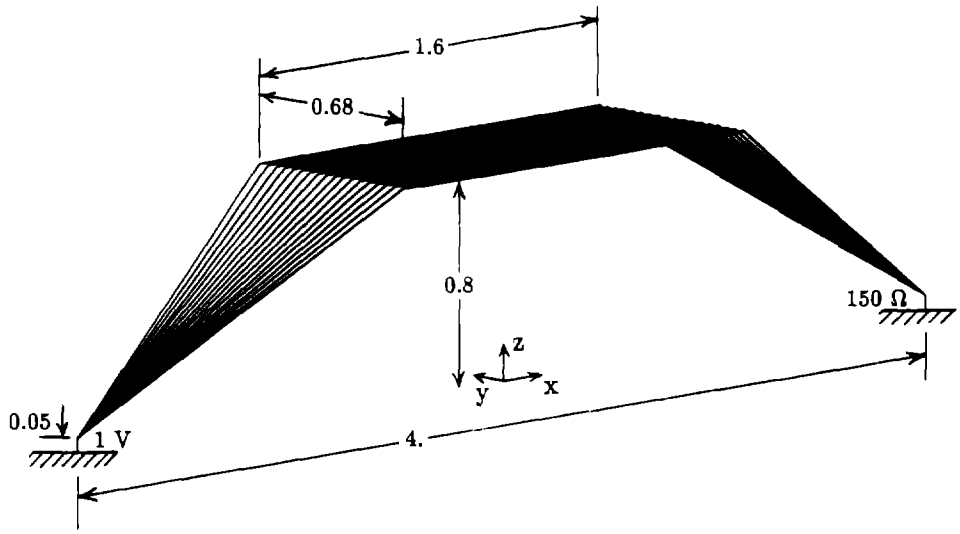

Fig. 10. Strip-line EMP simulator constructed from 18 wires. The line is driven by a voltage source against the ground plane with the other end terminated in a 150 ohm load. Dimensions are in meters, and the wire radius is 0.0008 m.

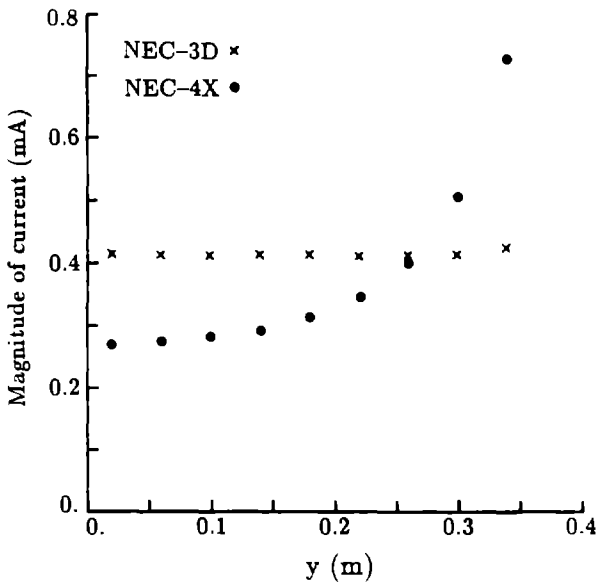

Fig. 11. Magnitude of current on the wires of the strip-line EMP simulator. Current is computed at a point 0.4 m from the center of the simulator toward the source.

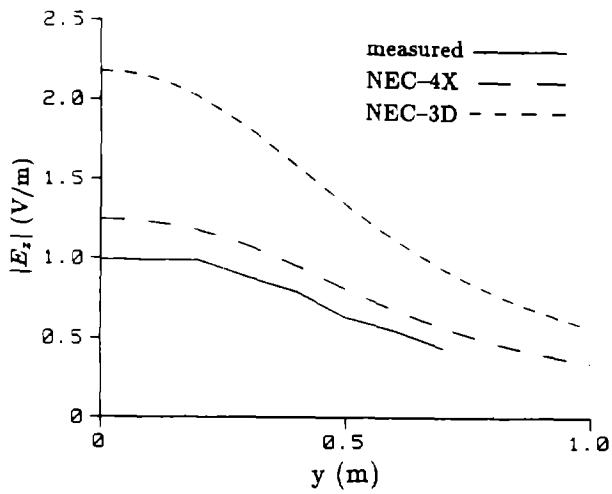

Fig. 12. Vertical electric field in the $z = 0.4$ m plane of the strip-line EMP simulator. NEC-3D, NEC-4X and measured values from [17] are compared.

4.4 A Model for Insulated Wires

A capability for modeling wires with thin insulating sheaths, in air or buried in the earth, has been developed in a version of NEC-3 known as NEC-3I [18]. The field due to radial polarization currents in the sheath is included in enforcing the boundary condition on the wire, as was done by Richmond and Newman in [19]. For a wire with radius a and sheath radius b, as shown in Fig. 13, the insulating sheath with complex relative permittivity $\tilde{\epsilon}_2 = \epsilon_2 - j\sigma_2/\omega\epsilon_0$ in a medium with $\tilde{\epsilon}_1 = \epsilon_1 - j\sigma_1/\omega\epsilon_0$, is replaced by an equivalent polarization current of

$$\vec{J}_s(\rho, z, \phi) = j\omega\epsilon_0(\tilde{\epsilon}_2 - \tilde{\epsilon}_1)[\vec{E}^S(\rho, z, \phi) + \vec{E}^I(\rho, z, \phi)], \qquad a \le \rho \le b$$

radiating in medium 1. $\vec{E}^S$ is the electric field due both to currents on the wire and to $\vec{J}_s$ itself, and $\vec{E}^I$ is the excitation field. To retain a one dimensional integral equation for the axial wire current, the sheath is assumed to be electrically thin, and the total field in the sheath is assumed to be dominated by the radial field due to charge on the wire. The polarization current is then

$$\vec{J}_s(\rho, z, \phi) \approx \frac{-(\tilde{\epsilon}_2 - \tilde{\epsilon}_1)}{2\pi\tilde{\epsilon}_2\rho} I'(z)\hat{\rho}, \qquad a \le \rho \le b.$$

In the thin wire approximation of the electric field integral equation, the field due to $\vec{J}_s$ is needed on the wire axis. For a straight segment of insulated wire with $|k_1 b| \ll 1$ the field on the axis due to $\vec{J}_s$ can be approximated, as shown in [18], in terms of the second derivative of the axial current as

$$\hat{z} \cdot \vec{E}_s^S(z) \approx \frac{j(\tilde{\epsilon}_2 - \tilde{\epsilon}_1)}{2\pi\omega\epsilon_0\tilde{\epsilon}_1\tilde{\epsilon}_2} I''(z)\ln(b/a) = \frac{-jk_s^2(\tilde{\epsilon}_2 - \tilde{\epsilon}_1)}{2\pi\omega\epsilon_0\tilde{\epsilon}_1\tilde{\epsilon}_2} C_i \ln(b/a).$$

where the final result is for the current distribution of Eq. (3). This field is included in the total, axial electric field in the thin-wire integral equation.

The field on the outside of the sheath due to the polarization currents in the sheath is shown in [18] to be less than this axial field by a factor of about $k_1^2(b^2 - a^2)/4$. Hence this field can be neglected relative to the axial field for thin wires, so that the mutual interaction of segments involves only the field due to the axial wire current. The model for the sheath thus reduces to a simple form comparable in complexity to the model for a wire with finite conductivity, in that the sheath modifies the field only on its own segment. This result is particularly convenient in the case of a wire near the air-ground interface since no addition is needed to the present evaluation of the effect of the interface on the field due to the axial wire current.

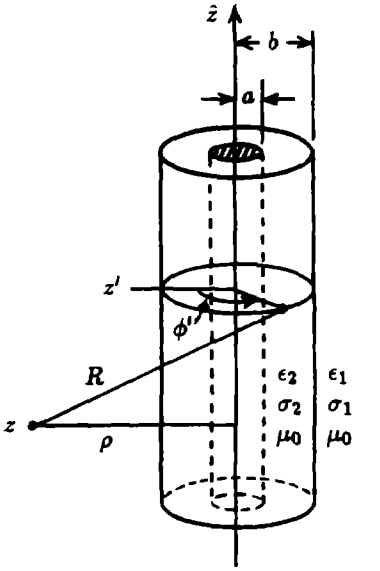

Fig. 13. Coordinates for evaluation of the field due to polarization currents in an insulating sheath on a wire.

One other change was needed in NEC to model insulated wires embedded in earth or water. In this case the current tends to have a sinusoidal form, as for a bare wire, but the wave number may be orders of magnitude less than for a bare wire in the medium. Use of k_s in Eq. (3) equal to the wave number in the surrounding medium can then result in very slow convergence of the solution. Fortunately, a simple approximation for the wave number on a buried insulated wire is available from the theory of coaxial transmission lines [20]. For a perfectly conducting wire, this solution predicts a wave number of

$$k_L \approx k_2\left[1 + \frac{H_0^{(2)}(k_1 b)}{k_1 b \ln(b/a) H_1^{(2)}(k_1 b)}\right]^{1/2} \tag{7}$$

where k_1 is the wave number in the infinite medium and k_2 is the wave number in the insulating material. $H_0^{(2)}$ and $H_1^{(2)}$ are Hankel functions of order 0 and 1. This approximation should be valid for $|k_1| \gg |k_2|$. Hence, in the NEC solution, k_s is set equal to k_L when $|k_1/k_2|$ is greater than 2. For smaller $|k_1/k_2|$, k_s is set equal to k_1. The accuracy of this estimate of k_s, within a factor of 2 or so, is not important since the solution is relatively insensitive to k_s. With a dense outer medium, the use of k_L in the current expansion greatly improves the convergence of the solution.

Allowing k_s different from k_1 increases the complexity of the field equations, however. The fields due to $\sin k_s s$ and $\cos k_s s$ current distributions, which are given by simple closed-form expressions when $k_s = k_1$, involve additional exponential integrals when $k_s \neq k_1$. The integrals were evaluated in NEC-3I by numerical integration after subtracting integrable functions to remove the peaked behavior of the integrand. Evaluation of these integrals can be difficult since, while $k_s\delta$ must be small, $k_1\delta$ may be large when $|k_1| \gg |k_2|$. The present evaluation appears to be accurate, but more work in this area could reduce the computation time.

To validate the insulated wire model in NEC, results were compared with published measurements for insulated antennas in air and water and with the solution for the propagation constant on an infinite insulated wire. The measured input admittance of a dipole antenna with dielectric insulation in air was included in [19]. NEC results are compared with these measurements and with the results of Richmond and Newman's code in Fig. 14. The two computer codes are in close agreement for the dipole antenna, with a difference evident only toward antiresonance, as often occurs with method-of-moments codes. Comparison with NEC results for a bare dipole showed that the resonant length was reduced from $0.47\lambda_0$ to $0.42\lambda_0$ by addition of the sheath. A similar comparison for a square loop is included in [18].

A valuable check on the NEC results is provided by the analytic solution for the propagation constant on an infinite insulated wire. A rigorous solution to this problem was developed by J. R. Wait [21] who solved the boundary value problem for a horizontal insulated wire buried in the ground below an interface with air. The wire is at depth d below the air-ground interface in a medium where the

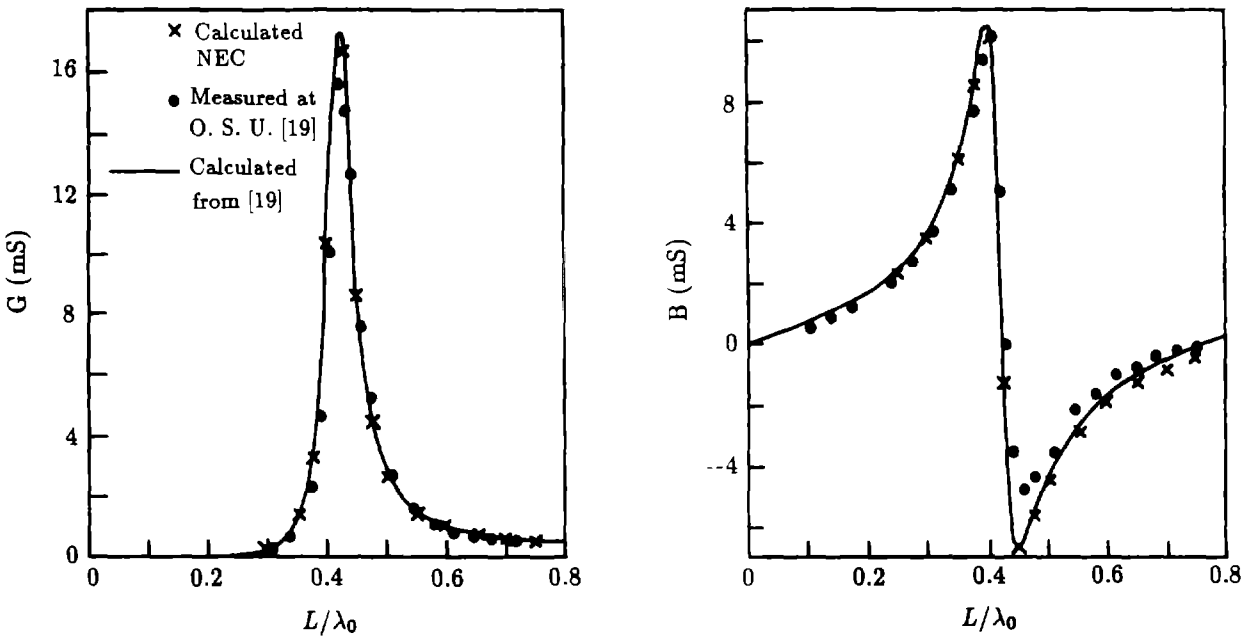

Fig. 14. Input admittance of an insulated dipole antenna in air with length L, radius $a = L/640$ and sheath radius $b = 5.84a$. The relative permittivity of the sheath is 2.3 and the conductivity is zero.

wave number is k_1 in the present notation. Assuming a current $I_0 \exp(-\Gamma x)$, Wait matched boundary conditions at the air-ground interface, the outer boundary of the sheath and on the wire, assuming that $d \gg b$ so that azimuthal variation of the field around the wire can be neglected, to derive an equation for Γ. An explicit solution for Γ is obtained in [21] when $|k_1| \gg |k_2|$. We chose here to solve Eq. (11) in [21] with a numerical root finder to ensure good accuracy over a wide range of parameters.

The transmission line model used in [20] provides another solution for the propagation constant on a buried insulated wire, which is repeated here as Eq. (7). An extension of this model to include an interface was proposed in [22] assuming an image of the wire reflected in the interface with a reflection coefficient of one. The result for a wire at depth d is

$$k_L = -j\Gamma \approx k_2 \left[1 + \frac{H_0^{(2)}(k_1 b) + H_0^{(2)}(2k_1 d)}{k_1 b \ln(b/a) H_1^{(2)}(k_1 b)} \right]^{1/2} . \tag{8}$$

As with Eq. (7) it is required that $|k_1| \gg |k_2|$ in this result.

To determine the propagation constant from the NEC solution, an insulated wire several wavelengths long was modeled with a source approximately $\lambda/4$ from one end and a load approximately $\lambda/4$ from the other end, where λ should be the wavelength of the propagating wave on the wire. The position and size of the terminating load were adjusted to achieve a reasonably small standing wave. This required some trial and error since the value of λ and the optimum load value were not known in advance. The phase constant β_L for the current was then determined from the phase shift divided by distance and the attenuation constant α_L was determined from a linear match to the log of the magnitude of current. The source and termination regions were excluded in these calculations.

The propagation constants determined from the NEC-3I solution, Eq. (7) or Eq. (8) and the solution from [21] are compared for a number of cases in [18]. For an infinite medium the wire radius a was varied with b/a fixed. A typical result for a wire with air insulation in conducting water is shown in Fig. 15. Wait's solution from [21] should be the most accurate of these results over the entire range of a/λ_0. The NEC solution is seen to be in good agreement with the result from [21] for small a/λ_0, diverging for larger values. The result of Eq. (7) is more accurate for large a/λ_0. Other results showed, as expected, that Eq. (7) becomes more accurate with increasing $|\tilde{\epsilon}_1|$. It is less accurate for small b/a and small $k_1 b$. Hence the NEC solution and Eq. (7) are often complementary in their ranges of accuracy. The value of α_L is more difficult to determine accurately than that of β_L for either Eq. (7) or NEC.

The input admittance computed by NEC-3I for an insulated monopole in conducting water with $\tilde{\epsilon}_1 = 80 - j0.197$ is compared in Fig. 16 with measurements made by S. Mishra and included in [20] and [23]. As described in [23], the monopoles were constructed from coaxial cable and were measured in lake

water at 300 MHz. Agreement is generally good in this case, with the NEC–3I results differing mainly in the height of the peak at resonance. Other cases included in [18] show increasing error in the peak heights for NEC–3I as b/a is increased, but good agreement in the resonant frequency. This observation confirms the results for the propagation constant on this monopole, for which $a = 3.175(10^{-3})\lambda_0$ and $k_1 b = 0.45$, since α_L from the NEC–3I solution is starting to diverge to large values while β_L is still reasonably accurate. Eq. (7) is accurate in this case but loses accuracy for smaller a/λ_0. Hence for smaller wire and sheath radii the NEC–3I solution should become more accurate and the the transmission line model less accurate.

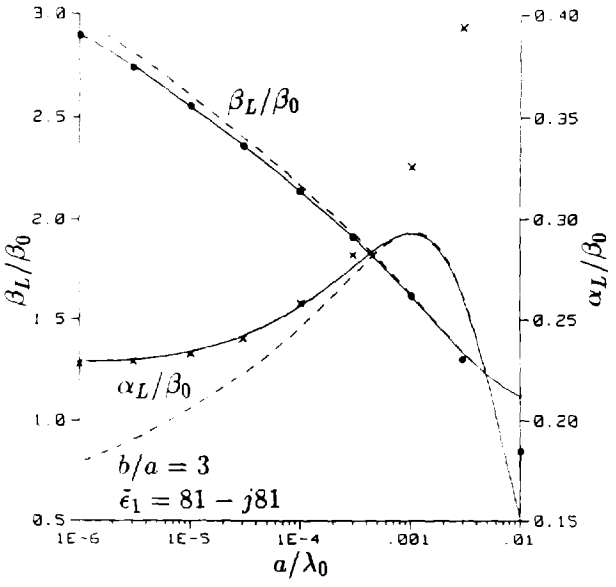

Fig. 15. Propagation constant $\Gamma = \alpha_L + j\beta_L$ versus wire radius a on a wire with air insulation in water with complex relative permittivity $\tilde{\epsilon}_1$ for $b/a = 3$ and $\beta_0 = 2\pi/\lambda_0$. Results of the NEC model (• ×) and Eq. (7) (– – – –) are compared with the more accurate solution from ref. [21] (———).

The propagation constant on an insulated wire near an interface as determined by NEC–3I was compared with that predicted by J. R. Wait's solution in [21] and with Eq. (8). Results from NEC–3I using the Sommerfeld integral option are compared in Fig. 17 with the solution from [21]. The latter, since boundary conditions are accurately satisfied at the interface, should be equivalent to the Sommerfeld integral solution. The results for β_L are seen to be in very good agreement, while α_L shows some difference for small d but generally good agreement. The maximum error in α_L is about 5 percent.

NEC–3I results using the reflection coefficient approximation are compared in Fig. 18 with the results of Eq. (8) which also is based on a reflection coefficient treatment of the interface. The two results are in reasonably good agreement but differ substantially from the presumably accurate results in Fig. 17. Hence it appears that the plane-wave reflection coefficient is not suitable for modeling a buried wire. Although the reflection coefficient is close to one for a dense ground, the cancellation in the integral for the field appears to require a more accurate treatment.

The comparisons with measurements and other analytic results indicate that the accuracy of the NEC model for an insulated wire in a conducting medium is mainly dependent on $|k_1 b|$. The error in α_L determined by NEC reaches ten percent when $|k_1 b|$ is approximately 0.15, while the solution for β_L, reaches ten percent error at about $|k_1 b| = 0.7$.

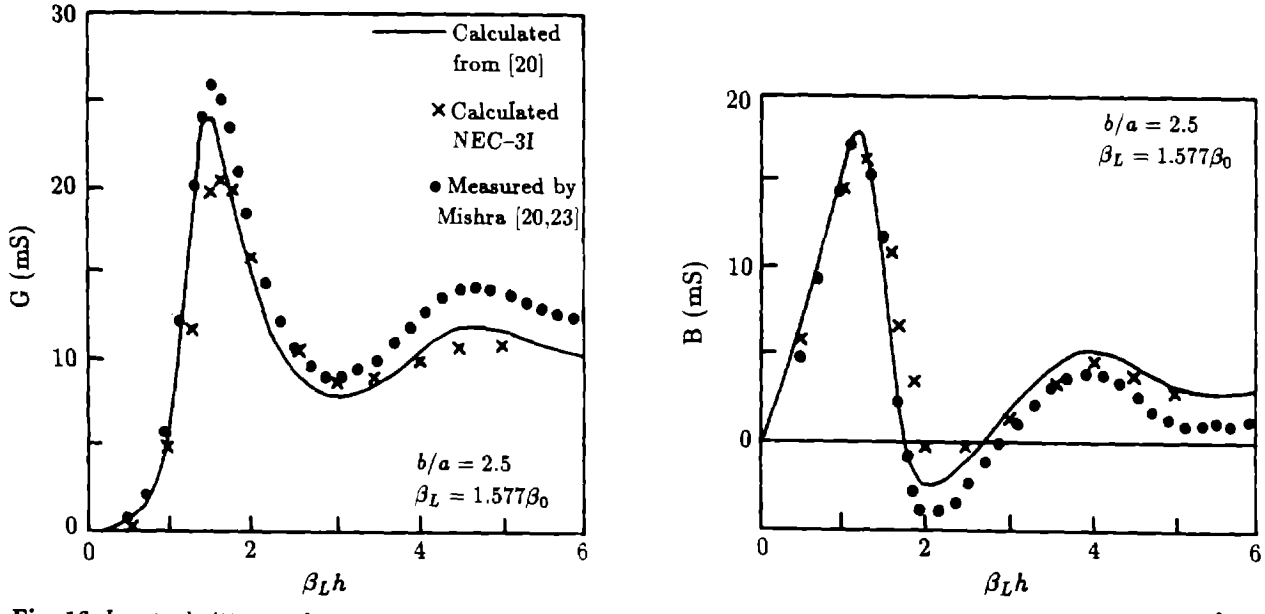

Fig. 16. Input admittance of a monopole antenna with air insulation in water with $\tilde{\epsilon}_1 = 80 - j0.197$ and $a = 3.175(10^{-3})\lambda_0$. The monopole height is h and β_L is the real part of k_L from Eq. (7).

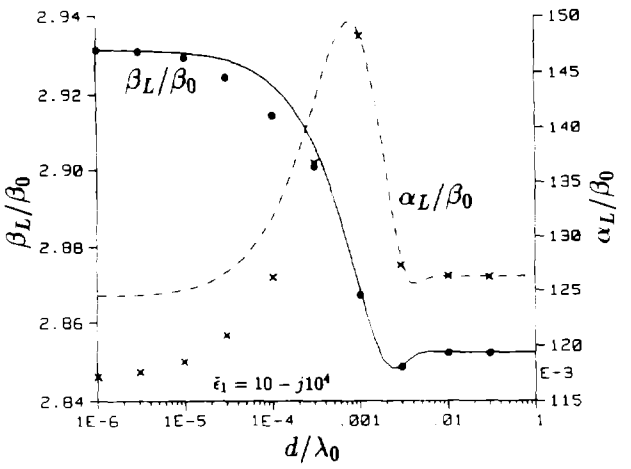

Fig. 17. Propagation constant on an insulated wire at depth d below an interface computed with the Sommerfeld integral option in NEC (• ×) and solution from [21] (——, - - -). The upper half space is air, the complex relative permittivity of the medium surrounding the wire is $\bar{\epsilon}_1$ and the insulation is air. Wire radius is $a = 2.38(10^{-7})\lambda_0$ with $b/a = 3$ and $\beta_0 = 2\pi/\lambda_0$.

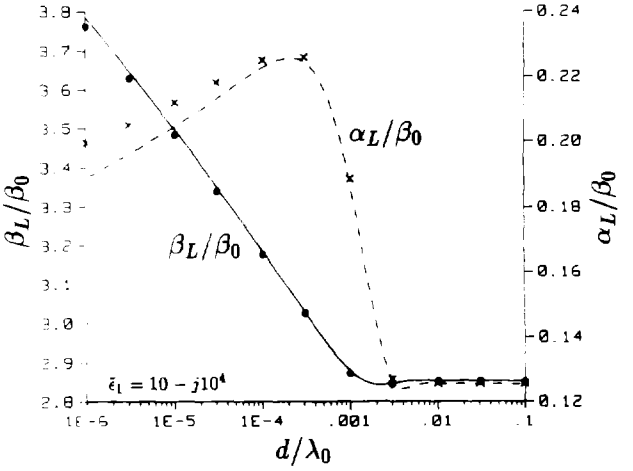

Fig. 18. Propagation constant on an insulated wire at depth d below an interface from the reflection coefficient option in NEC (• ×) and Eq. (8) (——, - - -). Both results are incorrect as a result of using the reflection coefficient for the interface. Model parameters are the same as for Fig. 17.

4.5 A Hybrid of NEC-MoM and GTD

Electrically large structures, in particular those composed of surfaces, are often modeled by means of the Geometrical Theory of Diffraction (GTD), since the moment method is limited by computation time and storage. A general purpose modeling code based on GTD/UTD has been developed at the Ohio State University [24], and is known as NEC-BSC. Development of this code is continuing, with a recent version described in [25]. It can model structures composed of combinations of conducting plates, multiple elliptic cylinders, multiple sectioned cone frustums, composite finite ellipsoids, and has a limited dielectric plate capability.

Since resonant sized antennas are often affected by large conducting bodies, either through near-zone interaction or distortion of the radiation patterns, a combination of the moment method and GTD/UTD approach is suggested. This hybrid technique was demonstrated by Thiele and Newhouse [26]. A code combining NEC-3 and NEC-BSC has been developed to test the practicality of the hybrid on a larger scale [27]. The main program of NEC-BSC was converted to a subroutine that can be called in three modes: 1) to read input data for the GTD model; 2) to evaluate the field at a point due to an arbitrarily oriented point current source; and 3) to evaluate the field in a given direction due to a point source. The moment-method code NEC-HYBRID calls NEC-BSC in mode 2 in filling the interaction matrix, and in mode 3 in computing the radiation pattern. Wires can be located anywhere permitted by the GTD restriction that distance from an edge be greater than about $\lambda/4$. NEC wire models may connect to the ground plane, since the full near field of the image is computed by NEC, but not to other surfaces in the GTD model for which only the $1/R$ field is evaluated.

Results of the NEC-HYBRID code for a monopole on a 90 degree wedge are shown in Fig. 19. The difference in input resistance from that of the monopole on an infinite ground plane, R_∞, is shown. The value of R_∞ determined by NEC-3 was 50.0 ohms, while for Thiele and Newhouse it was 53.3 ohms. The difference in the radiation patterns appears to be due to inaccuracy in the early results from [26].

Other auxiliary field evaluation routines could be adapted to link with the modified NEC-3 in place of NEC-BSC. For example, a simple wedge diffraction code has been used for fast evaluation of a wire on an infinite wedge. When the wedge in Fig. 19 was modeled with two large but finite plates in NEC-BSC, the time to fill the moment-method matrix was 15 times that for the monopole on an infinite ground plane. With the wedge diffraction code, the factor was only 2.

The hybrid approach could be extended to permit modeling the effect of terrain features on antenna radiation. Such features as hills or cliffs often have little effect on the antenna current or input impedance, affecting only the radiation pattern. At high frequencies, when only the space wave is of interest, terrain effects have been modeled by knife-edge diffraction, developed in the classic paper of Schelleng et al. [28] and later work, or by wedge diffraction modified for conductor loss [29]. At lower frequencies, propagation over terrain varying in height or conductivity has been modeled by solution

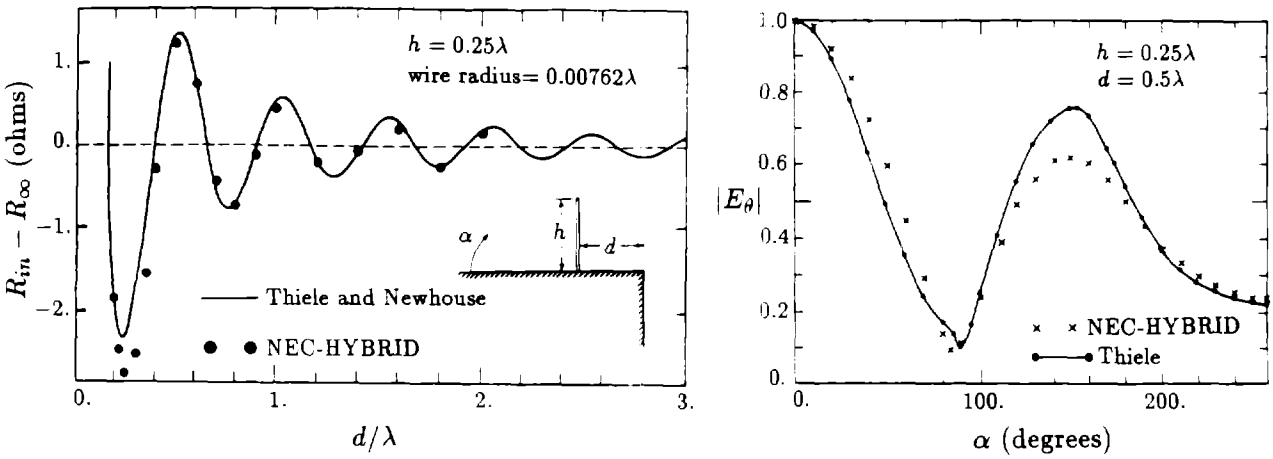

Fig. 19. Input resistance and radiation pattern of a monopole on a 90° wedge. NEC-HYBRID results are compared with those of Thiele and Newhouse [26].

of an integral equation [30]. Such propagation models can either be combined with the NEC code or used alone with input of currents from the NEC solution.

5. VALIDATION AND APPLICATIONS

Validation of a code such as NEC is an essential part of code development, and also must be a continuing consideration as the code is used in new applications. Errors, as discussed in [31], can be separated into physical modeling errors, which result from the approximations needed to represent a real structure in a form compatible with the numerical model; and numerical modeling errors, which result from approximations in the solution for the idealized model. Physical modeling errors generally must be assessed by the code user, based on understanding of physical principles or measurements. Numerical modeling errors can be evaluated by comparisons with measurements or independent analytical or numerical models, or often from self-consistency checks within the code.

Perhaps the most desirable form of validation is comparison with accurate measured results. However, measurement errors and uncertainties, and the difficulty of varying parameters in a physical model can limit the usefulness of this approach. Comparisons with independent analytical or numerical models also provide useful validation. An advantage of the latter approach is the ease of comparing over a wide range of parameters and the absence of random errors. However, one must be careful of approximations shared by the two models.

Self-consistency checks within a code such as NEC also are useful. An antenna result with negative input resistance is quickly recognized as indicating trouble. The balance of input and radiated power provides a test that is necessary, although not sufficient, to establish solution accuracy. The use of this test, in the form of average gain, was demonstrated in Table 1. Reciprocity of transmitting and receiving patterns or bistatic scattering provides a similar check. Although reciprocity may be guaranteed in a Galerkin method-of-moments solution, this is not the case in NEC. A valuable, although more computationally demanding, test is to evaluate the electric field along the surface of wires. The field will always be small at the match points if the matrix equation is being solved correctly. Usually errors in the field evaluation, basis functions or poor convergence in the model will be revealed by increased field between the match points.

Some validation tests performed with NEC are shown in the following figures. The radiation pattern of a cylinder with two attached wires in Fig. 20 demonstrates the hybrid EFIE-MFIE capability. The cylinder height is 22 cm, the diameter 20 cm, and the wire dimensions are shown on the figure. Wire a was driven by a voltage source

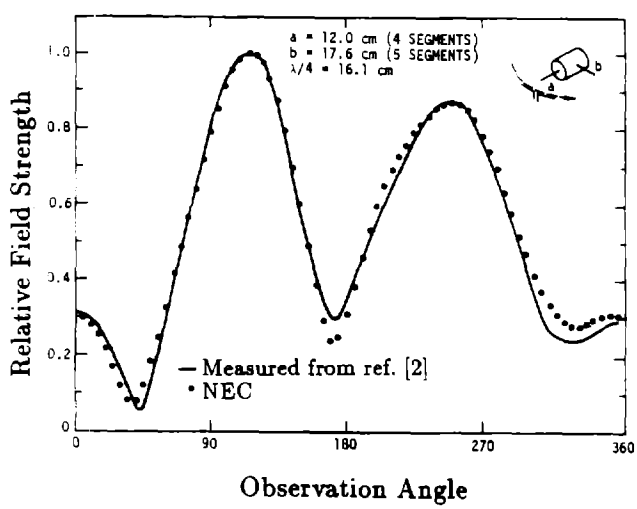

Fig. 20. Radiation Pattern of a cylinder with attached wires, with wire a excited.

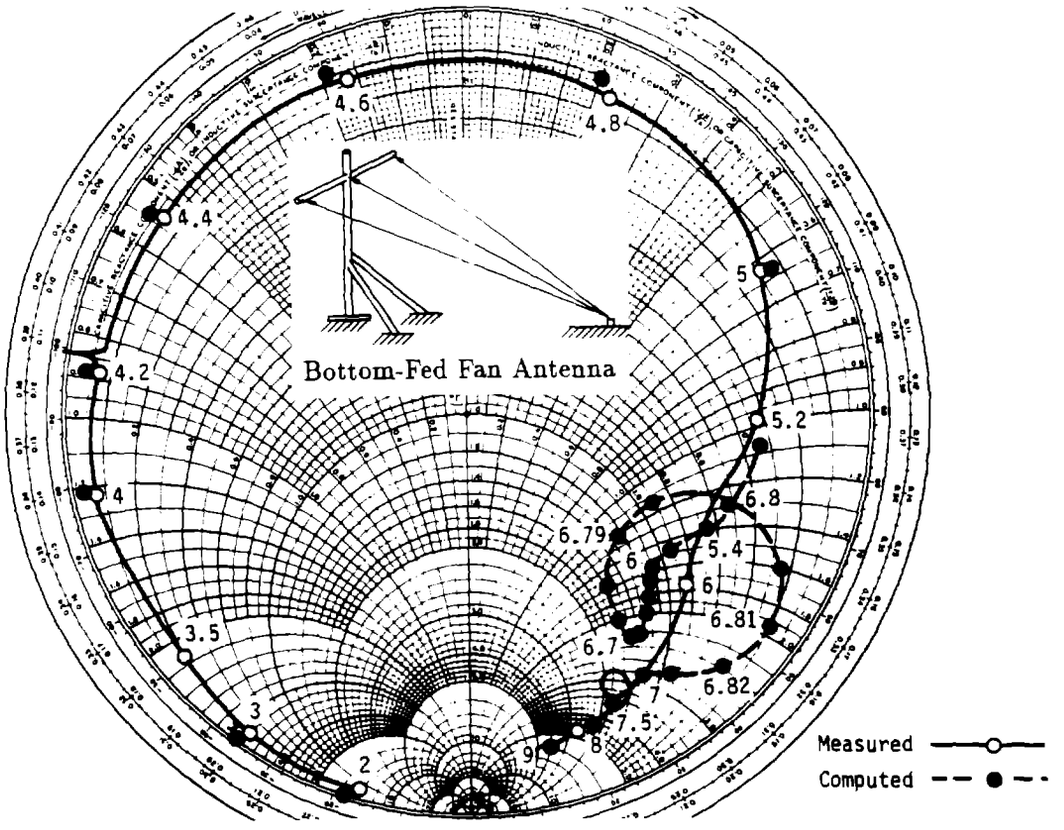

Fig. 21. Input impedance of a bottom-fed fan antenna. NEC results are compared with measurements from the Naval Ocean Systems Center on a 1/24 scale model. Frequencies are shown in MHz.

at its base, while wire *b* was connected directly to the cylinder. The measured pattern was obtained by Albertsen et al. [2] who presented similar numerical results. NEC results for a higher density of patches than was used for Fig. 20 were in worse agreement with the measurements, indicating possible problems in convergence of the MFIE solution for a surface with square edges.

The computed input impedance of a bottom-fed fan antenna is compared with measurements in Fig. 21. This result from [32] is one of several validation exercises performed for antennas used on ships [33,34]. The results for the fan are generally in good agreement from 2 to 9 MHz. However, the NEC results show a loop on the Smith chart from 6.7 to 7 MHz that does not correspond to the smaller loop in the measurements. Examination of the currents showed that this behavior was due to a transmission line-mode resonance in the wires of the fan. Such a phenomenon can be very sensitive to the exact dimensions of the structure and conductivity of the wire and insulators. The NEC model assumed perfectly conducting wires and an air gap for the insulators which may account for this difference.

The results in Fig. 21 were obtained with the three wires of the fan driven by three separate voltage sources against the ground plane. An alternate model would be to connect the three wires to a short vertical segment on which the source is located. Results in [32] for the single-source model were in worse agreement with measurements than those in Fig. 21, however. They showed a frequency shift of up to ten percent at the lower frequencies and negative input resistance over part of the transmission-line resonance around 7 MHz. However, when the single-segment source is run in the new code NEC–4X, described in Section 4.3, the results are close to those in Fig. 21. Hence the treatment of charge at the junction is the apparent source of error in NEC–3.

Verification of accuracy is a particular concern when modeling antennas over a finitely conducting ground due to the complexity of the ground model. As discussed in [8], internal checks such as integrating the total radiated power for a dielectric ground, and numerical checks on boundary conditions along wires or across the interface were quite useful for validation. NEC–3 was in good agreement with an independent moment-method code for a vertical cylinder passing through the interface with no *a priori* condition on charge density [35].

The wave number for current on a horizontal wire over the ground provides a test that is sensitive to the accuracy of the ground model and can conveniently be compared with analytic solutions. Such a comparision for a buried insulated wire was demonstrated in Figs. 17 and 18. For a bare wire above

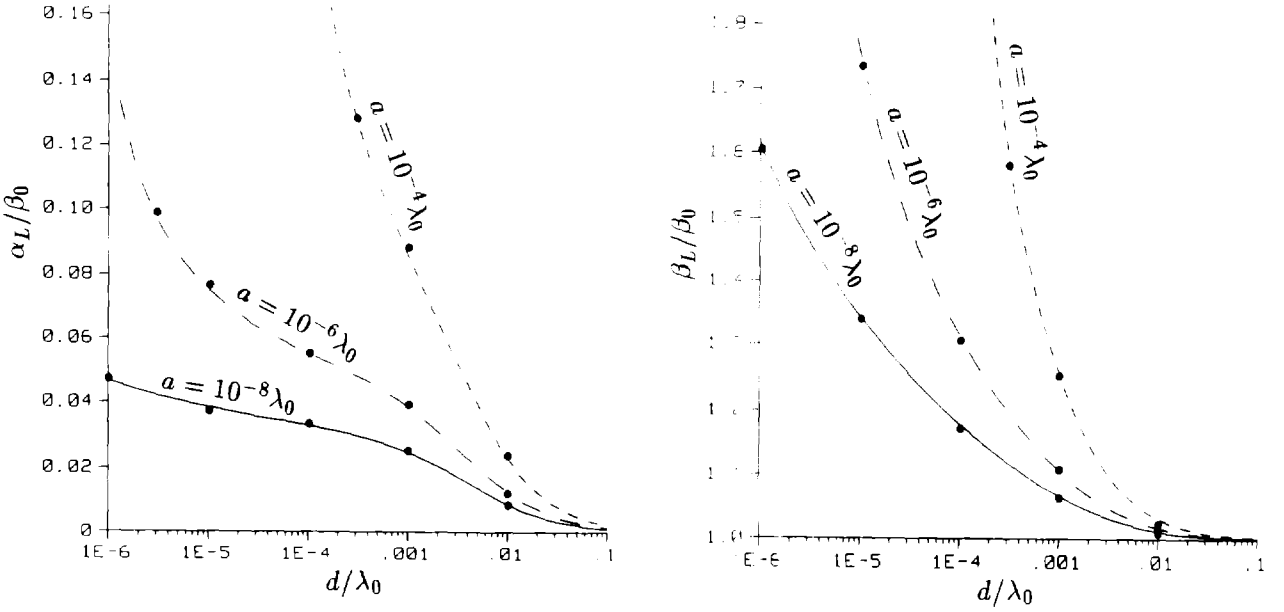

Fig. 22. Wave number $k_L = \beta_L - j\alpha_L$ on a horizontal wire with radius a at height d above a ground plane. NEC results (points) are compared with results of the eccentrically insulated transmission line model (lines) from [36].

ground, an approximation for the wave number was derived in [36] from the equations for a coaxial transmission line with lossy outer conductor and eccentrically located inner conductor. The outer conductor radius is allowed to go to infinity so that the transmission line becomes a wire at height d above a flat ground plane. Approximations in this model require that the wave number in the ground be much greater than that in the medium surrounding the wire. The propagation constant from this formula has been compared with measurements for a wire over water with good agreement [37].

The wave number k_L determined from NEC is compared with that from the transmission line approximation in Fig. 22 for a ground with $\bar{\epsilon}_g = 10 - j1000$ and for wire radii of $10^{-8}\lambda_0$, $10^{-6}\lambda_0$ and $10^{-4}\lambda_0$. This complex relative permittivity would correspond to a reasonably good ground ($\sigma = 0.01$ S/m) at about 200 kHz. The agreement is seen to be very good for this case. For lower ground conductivity the transmission line approximation would lose accuracy, while NEC would be expected to remain accurate.

The results in Fig. 22 represent a test of the accuracy of the field evaluation very near the interface. Another critical factor in the ground model is the treatment of charge on wires passing through the interface or junctions near the interface. This was a particular concern in a special version of NEC–3 (NEC–GS) developed to model a monopole on a uniform radial-wire ground screen. By taking full advantage of the physical symmetry and excitation symmetry, NEC–GS can model large radial-wire screens in much less time and storage than would be required by NEC–3. Little accurate experimental data is available for comparison, however, so validation has relied on self-consistency checks such as convergence and power balance. Also, a comparison with an approximation developed by Wait and Pope [38] has helped to validate the NEC–GS results.

In the NEC model for a ground screen, the junction is located exactly on the interface with the first segment on each radial sloping downward to the desired depth of the screen. One question in this model was the treatment of charge at the junction of the monopole and the radial wires, where many wires meet with narrow angles of separation. In the current expansion, the derivative of current on the monopole just above the interface (I'_+) and on the radials below ground (I'_-) is made to satisfy the condition $I'_-/I'_+ = \bar{\epsilon}_g$, where $\bar{\epsilon}_g = \epsilon_- - j\sigma_-/\omega\epsilon_0$ is the complex relative permittivity of the ground. This condition was derived for continuity of radial electric field of a vertical wire penetrating the interface [8], so its application to the ground screen could be questioned.

Results for buried ground screens are generally found to be stable with varying segment lengths, however. The most difficulty has been encountered in modeling ground screens floating above the ground. In this case, since all wires are in air, the charge densities on wires at the junction are forced to be equal for equal wire radii. To obtain converged results for ground screens at small heights above the ground, it was necessary to use segment lengths at the junction on the order of the height of the screen above ground, tapering to larger segments away from the junction . This is particularly important for

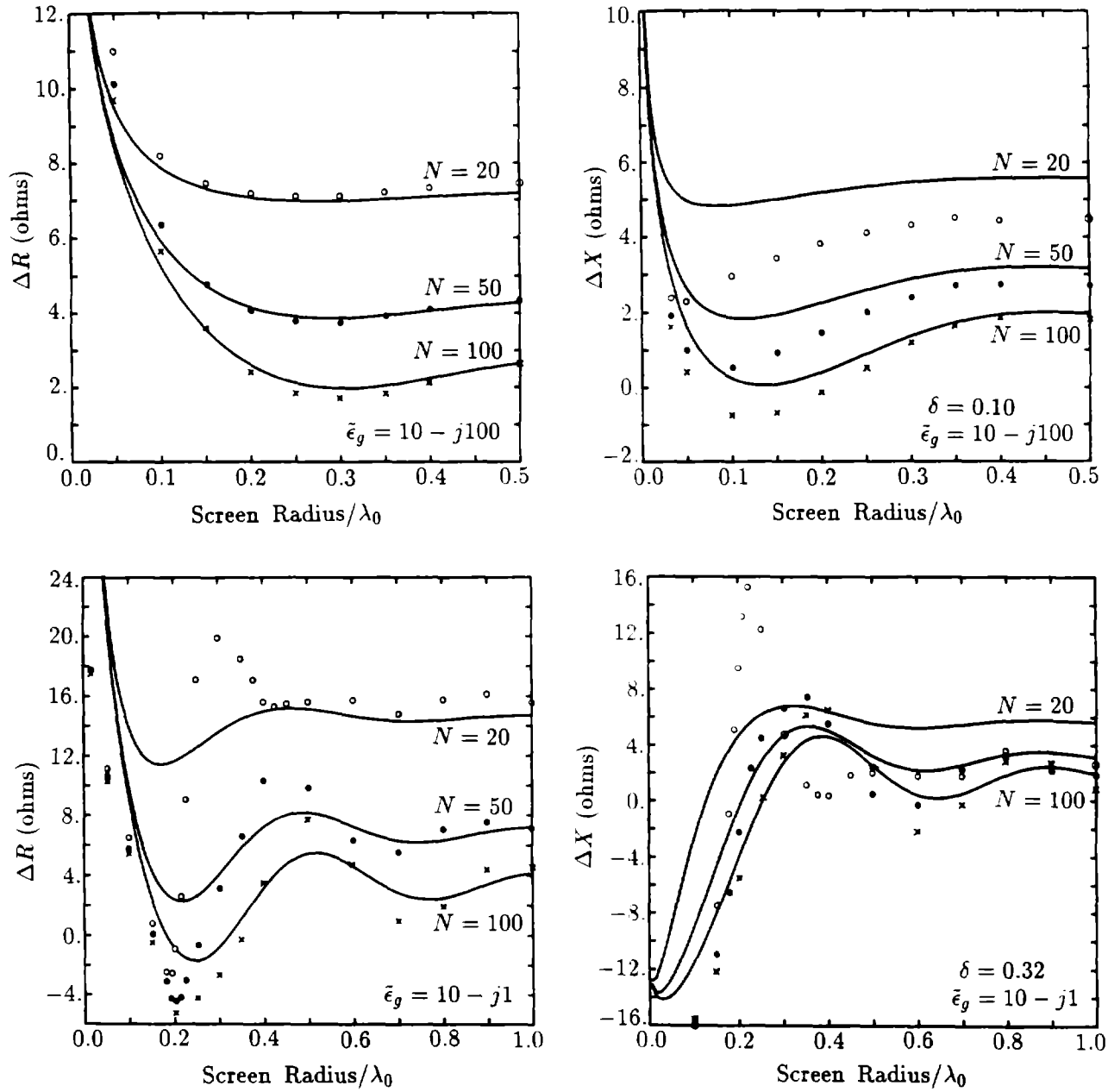

Fig. 23. Input impedance of a $\lambda/4$ monopole on a buried radial wire ground screen with N wires, showing the difference from the impedance on a perfectly conducting ground plane. NEC results (points) are compared with results from a result derived from the compensation theorem [38].

electrically small monopoles and screens. A treatment of charge similar to that described in Section 4.3, but taking the ground into account, appears necessary to obtain an optimum basis function.

As a check on the solution for buried ground screens, the computed input impedance of a monopole was compared with that predicted by an approximation developed by Wait and Pope [38]. For this approximation, a current $I_0 \cos(kz)$ is assumed on the monopole. The difference in input impedance (ΔZ) between that of the monopole on the radial-wire screen in real earth and that of the monopole on an infinite perfectly conducting ground is obtained as an integral over the surface, through application of the compensation theorem. The magnetic field over the ground surface is taken to be that on the perfect ground, and the electric field is related to it by a surface impedance for the screen and ground, or for bare ground beyond the screen. A derivation of this approximation and results are included in [39]. Wait states that this approximation should be accurate for a screen radius in wavelengths (b/λ_0) somewhat greater than $\delta = |\tilde{\epsilon}_g|^{-1/2}$. Also, the number of wires in the ground screen must be sufficiently large for the surface impedance approximation to be valid.

The ΔZ computed by NEC-GS is compared with that from the compensation theorem result in Fig. 23. The input impedance computed by NEC-GS for the monopole on an infinite perfectly conducting ground was $38.6 + j22.2$ ohms. Agreement in ΔZ is generally good for b/λ_0 greater than δ. The

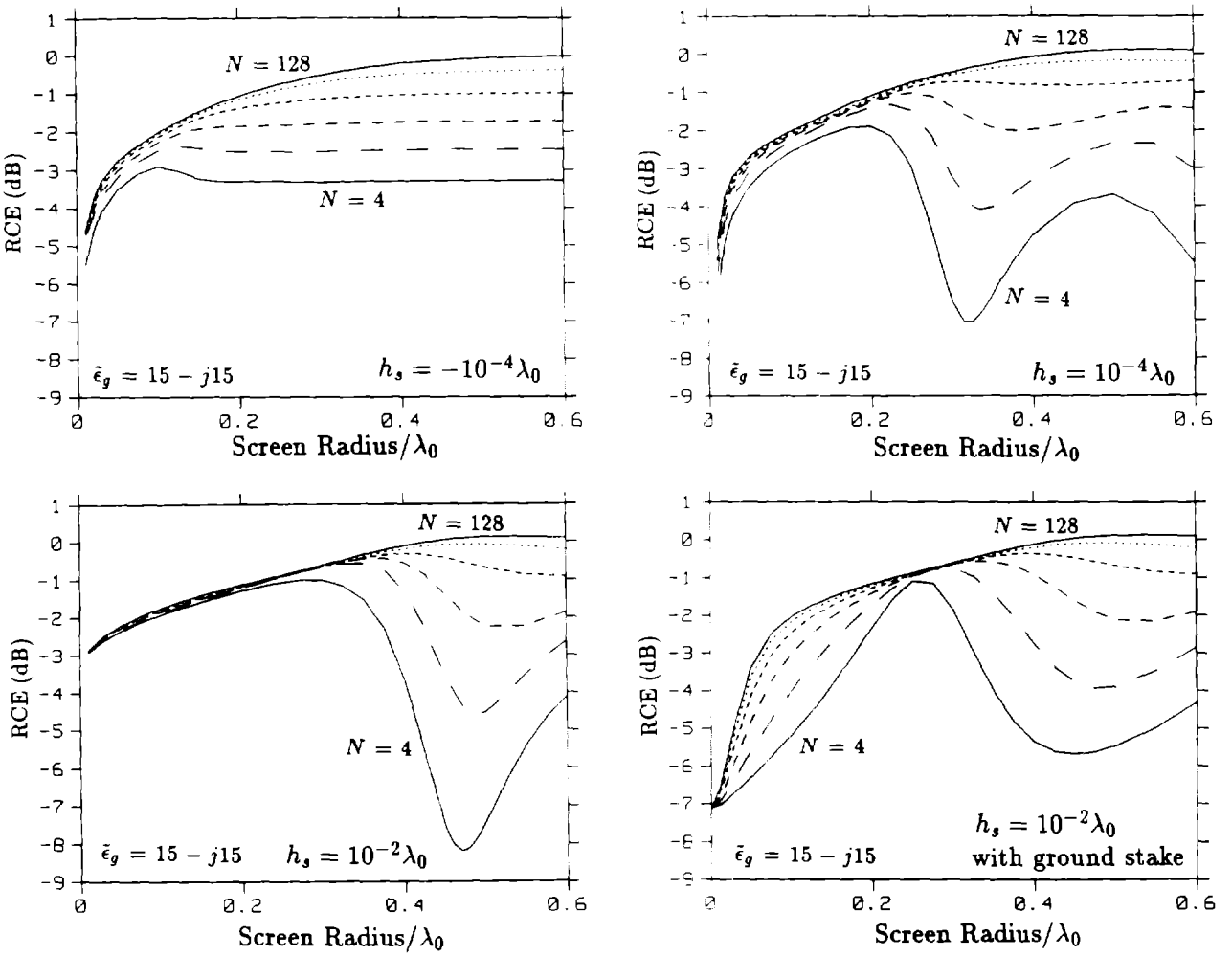

Fig. 24. Relative Communication Efficiency of a $\lambda_0/4$ monopole on a radial-wire ground screen below and above the surface of the ground. The height of the screen above the ground is h_s and the number of radials N is 4, 8, 16, 32, 64 and 128.

larger discrepancies for 20 radials are most likely due to failure of the surface impedance approximation for a sparse screen. The discrepancies for low ground conductivity are due to standing waves on the screen wires which are not taken into account by the compensation theorem solution. This comparison supports the accuracy of the NEC model, which should remain accurate for sparse screens and low ground conductivity. Unfortunately, the compensation-theorem result fails for small screen radius where the NEC model appears most in doubt.

Some results for antennas operated over ground follow to demonstrate the usefulness of the code for parametric studies. Fig. 24 shows the Relative Communication Efficiency (RCE) of a $0.25\lambda_0$ monopole on a radial-wire ground screen buried and above the ground. RCE is defined as the ratio of power density at some receiver location due to the test antenna to that due to a reference antenna for equal input powers. The reference antenna in this case was the monopole on a buried screen with 128 radials, and the receiver location was on the ground $1000\lambda_0$ from the transmitter.

While wires exactly on the interface cannot be modeled due to the thin wire approximation, the results for screens $10^{-4}\lambda_0$ below and above the ground surface are nearly the same for small screen radius, until current attenuation limits the buried screen. Sparse screens above ground show a sharp loss of efficiency when the radials are near to a half-wavelength resonance. For a screen height of $10^{-4}\lambda_0$ the interaction with the ground shifts this resonance down to where it reduces the RCE for four radials as short as $0.25\lambda_0$. Inclusion of a ground stake under the monopole, in addition to the radial-wire screen, is sometimes recommended, either to improve antenna performance or for safety. The last result in Fig. 24, in which the stake depth was $0.02\lambda_0$, and results for other grounds show mainly detrimental effects for the ground stake. Multiple shorter stakes were more effective but still reduced efficiency, especially for small screen radius. With lower ground conductivity, the buried screen was also affected by screen resonances, as shown in Fig. 25.

The RCE of a Beverage antenna is shown in Fig. 26 for varying length and height. In this case, the reference antenna used to normalize the results was a vertical dipole with length $0.1\lambda_0$ on the interface.

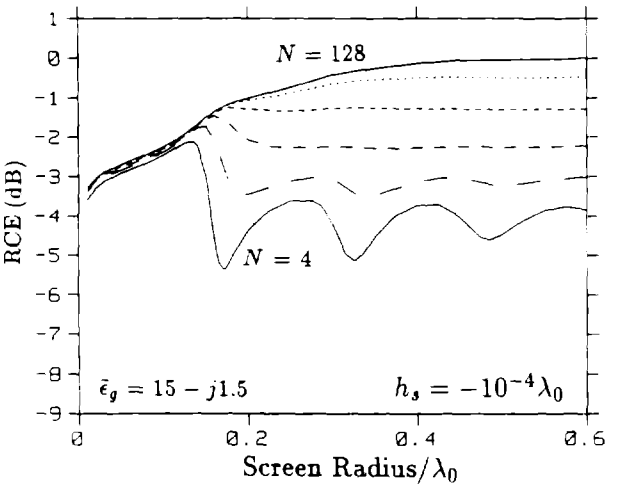

Fig. 25. Relative Communication Efficiency of a $\lambda_0/4$ monopole on a radial-wire ground screen buried by $10^{-4}\lambda_0$. The number of radials N is 4, 8, 16, 32, 64 and 128.

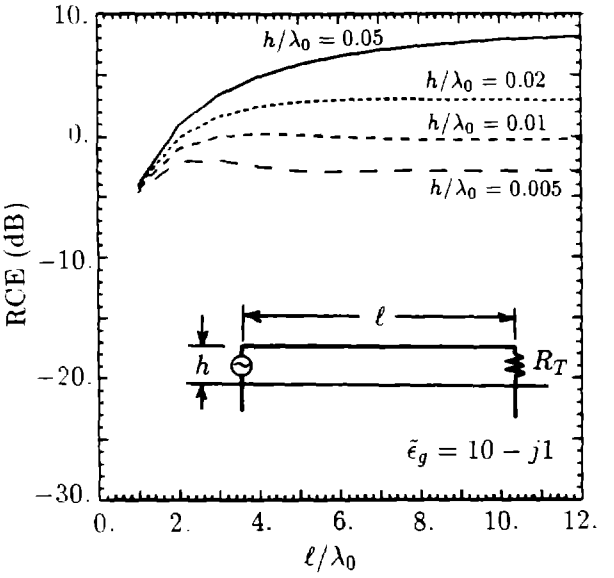

Fig. 26. Relative Communication Efficiency of a Beverage antenna for varying length, with height a parameter.

The limitation of gain due to phase lag along the wire is evident as the length is increased.

NEC has been applied to generate an antenna engineering handbook and data base [40]. This effort included basic field-antenna types: whips on ground stakes, screens and boxes; half-squares, vee beams, horizontal dipoles, inverted vee dipoles, long wires and loops. Tables of radiation patterns were generated for a range of frequencies and grounds

6. CONCLUSION

NEC is a versatile code for modeling antennas and their environment. It has become widely used, due mainly to its convenient operation, documentation, availability and continuing support. Recent extensions to NEC include a model for insulated wires and improved accuracy in modeling electrically small antennas and discontinuities in wire radius. Valuable extensions for future consideration include the addition of an EFIE model for open surfaces such as plates and a model for antennas in or over stratified ground. A longer range goal is to incorporate expert-systems technology to simplify the process of building models that conform to the modeling guidelines and to verify that the code is producing correct results.

The utility of NEC has been enhanced by the development of an interactive graphics utility (IGUANA) [41] for developing the model description and examining results. IGUANA supports both NEC and the moment-method code MININEC [13] for use on personal computers. A package NEEDS–1.0 is now available from the Applied Computational Electromagnetics Society (ACES) that includes NEC–2 for an IBM PC as well as IGUANA, MININEC and the GRAPS graphics package.

NEC is written in Fortran and consists of about 10,000 lines of code. Versions are available for DEC/VAX, CDC, CRAY and IBM, and it has been converted to a number of other computers. Of the versions currently being released, NEC–2 has no distribution restrictions, while NEC–3 and other versions in development require authorization from the U. S. Department of Defense.

The development of NEC has been sponsored by the U. S. Army ISEC (J. McDonald, L. Corrington) and CECOM (P. Cunningham) and the U. S. Navy NOSC (J. Logan, S. T. Li). The work to model insulated wires was partially sponsored by the U. S. Air Force, RADC/EECT and RADC/DCCL.

REFERENCES

[1] G. J. Burke and A. J. Poggio, *Numerical Electromagnetics Code (NEC) - Method of Moments*, Lawrence Livermore National Laboratory, Rept. UCID–18834, January 1981.

[2] N. C. Albertsen, J. E. Hansen and N. E. Jensen, *Computation of Spacecraft Antenna Radiation Patterns*, The Technical University of Denmark, 1972.

[3] A. J. Poggio and E. K. Miller, "Integral Equation Solutions of Three-Dimensional Scattering Problems," Chapt. IV in *Computer Techniques for Electromagnetics*, edited by R. Mittra, Pergamon Press NY, 1973.

[4] A. J. Poggio and R. W. Adams, *Approximations for Terms Related to the Kernel in Thin-Wire Integral Equations*, Lawrence Livermore National Lab. Rept. UCRL-51985, December 1975.

[5] R. F. Harrington, *Field Computation by Moment Methods*, McGraw Hill Book Company, New York, 1961.

[6] Y. S. Yeh and K. K. Mei, "Theory of Conical Equiangular Spiral Antennas," Part I – Numerical Techniques, *IEEE Trans. Antennas and Propagation*, Vol. AP-15, p. 634, 1967.

[7] T. T. Wu and R. W. P. King, "The Tapered Antenna and its Application to the Junction Problem for Thin Wires," *IEEE Trans. Antennas and Propagation*, Vol. AP-24, pp. 42-45, 1976.

[8] G. J. Burke and E. K. Miller, "Modeling Antennas Near to and Penetrating a Lossy Interface," *IEEE Trans. Antennas and Propagation*, Vol AP-32, No. 10, pp. 1040-1049, 1984.

[9] G. J. Burke, "Test of a Coaxial-Line Source Model for NEC," Proceedings of the 3rd Annual Review of Progress in Applied Computational Electromagnetics, Monterey, CA, March 24-26, 1987.

[10] G. J. Burke, *Enhancements and Limitations of the Code NEC for Modeling Electrically Small Antennas*, Lawrence Livermore National Laboratory, Rept. UCID–20970, January 1987.

[11] G. J. Burke, *Treatment of Small Wire Loops in the Method of Moments Code NEC*, Lawrence Livermore National Laboratory, Rept. UCID-21196, October 1987.

[12] D. R. Wilton, University of Houston, private communication.

[13] J. C. Logan and J. W. Rockway, *The New MININEC (Version 3): A Mini-Numerical Electromagnetic Code*, Naval Ocean Systems Center TD 938, September 1986.

[14] A. W. Glisson and D. R. Wilton, *Numerical Procedures for Handling Stepped-Radius Wire Junctions*, Department of Electrical Engineering, University of Mississippi, March 1979.

[15] A. C. Ludwig, "Wire Grid Modeling of Surfaces," *IEEE Trans. Antennas and Propagation*, Vol. AP-35, pp. 1045-1048, 1987.

[16] P. C. Waterman, "Matrix Formulation of Electromagnetic Scattering," *Proceedings of the IEEE*, Vol. 53, pp. 805-812, August 1965.

[17] J. P. Desmettre, Commissariat a L'Energie Atomique, France, Private Communication.

[18] G. J. Burke, *A Model for Insulated Wires in the Method of Moments Code NEC*, Lawrence Livermore National Laboratory, Rept. UCID-21301, January 1988.

[19] J. H. Richmond and E. H. Newman, "Dielectric Coated Wire Antennas," *Radio Science*, Vol. 11, no. 1, pp. 13–20, Jan. 1976.

[20] R. W. P. King and G. S. Smith, *Antennas in Matter*, The MIT Press, Cambridge, MA, 1981.

[21] J. R. Wait, "Electromagnetic Wave Propagation Along a Buried Insulated Wire," *Canadian J. of Phys.*, Vol. 50, pp. 2402-2409, 1972.

[22] R. W. P. King, "Antennas in Material Media Near Boundaries with Application to Communication and Geophysical Exploration, Part II: The Terminated Insulated Antenna," *IEEE Trans. Antennas and Propagation*, Vol. AP-34, no. 4, pp. 490–496, April 1986.

[23] R. W. P. King, S. R. Mishra, K. M. Lee and G. S. Smith, "The Insulated Monopole: Admittance and Junction Effects", *IEEE Trans. Antennas and Propagation*, Vol. AP-23, no. 2, pp. 172–177, March 1975.

[24] R. J. Marhefka and W. D. Burnside, "Numerical Electromagnetics Code – Basic Scattering Code, NEC–BSC (Version 2), Part I: User's Manual," Technical Report 712242-14, December 1982, The Ohio State University ElectroScience Laboratory, Department of Electrical Engineering; prepared under Contract No. N00123-79-C-1469 for Naval Regional Contracting Office.

[25] R. J. Marhefka, "Development and Validation of a New Version of the NEC–BSC," Proceedings of the 4th Annual Review of Progress in Applied Computational Electromagnetics, Monterey, CA, March 22-24, 1988.

[26] G. A. Thiele and T. H. Newhouse, "A Hybrid Technique for Combining Moment Methods with the Geometrical Theory of Diffraction," *IEEE Trans. Antennas and Propagation*, Vol. AP-23, pp. 62-69, January 1975.

[27] G. J. Burke, *NEC-HYBRID User's Guide*, Lawrence Livermore National Laboratory, Rept. UCID-20959, 1987.

[28] J. C. Schelleng, C. R. Burrows and E. B. Ferrell, "Ultra-Short-Wave Propagation," *Proceedings of the IRE*, Vol. 21, No. 3, March, 1933.

[29] R. J. Luebbers, "Propagation Prediction for Hilly Terrain Using GTD Wedge Diffraction," *IEEE Trans. Antennas and Propagation*, Vol. AP-32, No. 9, Sept. 1984.

[30] R. H. Ott and L. A. Berry, "An Alternative Integral Equation for Propagation over Irregular Terrain," *Radio Science*, Vol. 5, No. 5, pp. 767-771, May 1970.

[31] E. K. Miller, "A Selective Survey of Computational Electromagnetics," *IEEE Trans. Antennas and Propagation*, Vol. 36, No. 9, pp. 1281-1305, Sept. 1988.

[32] G. J. Burke and A. J. Poggio, *Computer Analysis of the Bottom-Fed Fan Antenna*, Lawrence Livermore National Laboratory, Rept. UCRL–52109, August 1976.

[33] G. J. Burke and A. J. Poggio, *Computer Analysis of the Twin-Whip Antenna*, Lawrence Livermore National Laboratory, Rept. UCRL–52080, June 1976.

[34] F. J. Deadrick, G. J. Burke and A. J. Poggio, *Computer Analysis of the Trussed-Whip and Discone-Cage Antennas*, Lawrence Livermore National Laboratory, Rept. UCRL–52201, January 1976.

[35] W. A. Johnson, "Analysis of a vertical, tubular cylinder which penetrates an air-dielectric interface and which is excited by an azimuthally symmetric source," *Radio Science*, Vol. 18, No. 6, pp. 1273-1281, 1983.

[36] R. W. P. King, T. T. Wu and L. C. Shen, "The horizontal wire antenna over a conducting or dielectric half space: current and admittance," *Radio Sci.*, Vol. 9, No. 7, pp. 701-709, 1974.

[37] R. M. Sorbello, R. W. P. King, K. M. Lee, L. C. Shen and T. T. Wu, "The horizontal wire antenna over a dissipative half-space: generalized formula and measurements," *IEEE Trans. Antennas and Propagation*, Vol. AP-25, No. 6, 1977.

[38] J. R. Wait and W. A. Pope, "The Characteristics of a Vertical Antenna with a Radial Conductor Ground System," *Appl. Sci. Res.*, Sec. B, Vol. 4, pp. 177-195, 1954.

[39] J. R. Wait, "Characteristics of Antennas Over Lossy Earth," Chapter 23 in *Antenna Theory:* Part II, ed. R. E. Collin and F. J. Zucker, McGraw Hill Book Co., Inc., New York, 1969.

[40] J. K. Breakall, E. E. Domning and A. M. Christman, *Antenna Engineering Handbook*, Lawrence Livermore National Laboratory, Rept. UCID-21271, 1987.

[41] J. Strauch and S. Thompson, *Interactive Graphics Utility for Army NEC Automation (IGUANA)*, Naval Ocean Systems Center, Rept. CR 308, 1985.

Technical Information Department • Lawrence Livermore National Laboratory
University of California • Livermore, California 94550